Measurement and Correction for the Magnetic Susceptibility Effects of Fat in Venous Oximetry: Application in the Quantification of Muscle Oxygen Consumption (VO_2) with Plantar Flexion Exercise

by

Hyun Joo Esther Yang

A thesis submitted in partial fulfillment of the requirements for the degree of

Master of Science

in

Biomedical Sciences

Department of Biomedical Engineering
University of Alberta

Abstract

Measuring venous oxygen saturation (SvO_2) provides direct assessment of the upstream muscle or organ's ability to extract and metabolize oxygen. Previously, measurement of venous oxygen saturation has been performed in most studies by intravenous catheterization. This approach has the advantage of continuous monitoring at the bedside, but the catheter insertion is an invasive method and has risks including venous infection and thrombosis.

Magnetic Resonance Imaging (MRI) has the potential to estimate the blood oxygen saturation level based on the difference of the magnetic properties of oxygenated and deoxygenated hemoglobin in the blood. While oxyhemoglobin is diamagnetic, deoxyhemoglobin is paramagnetic relative to the surrounding tissue which makes it possible to estimate venous oxygen saturation levels, which is termed oximetry.

In magnetic susceptometry-based oximetry, the vessel is modeled as a long paramagnetic cylinder immersed in an external uniform magnetic field. The resulting magnetic field shift within cylindrical blood vessels can be used to estimate venous oxygen saturation, based on the known magnetic susceptibility of deoxyhemoglobin. However, conduit veins in the periphery are often surrounded by fat, which has a different magnetic susceptibility than water and the venous blood pool. The potentially complex magnetic field perturbation from the fat may extend into the vein and the surrounding muscle reference tissue, potentially confounding estimation of the venous oxygen saturation.

In this thesis, new methods for the measurement and correction of the unwanted magnetic susceptibility effects of fat are explored, to enable magnetic susceptometry-based venous oximetry in the presence of large fat pools around the targeted veins. Compatibility with dynamic imaging in associated with plantar flexion (calf) exercise is evaluated. The addition of flow-encoding

gradients enable phase-contrast evaluation of venous blood flow in the same acquisition, which allow for direct calculation of the volume of muscle oxygen consumption, VO_2, which is the product of oxygen extraction and blood flow.

Preface

This thesis is an original work by Hyun Joo Esther Yang. The main research project, of which this thesis is a part, received research ethics approval from the University of Alberta Research Ethics Board, *Skeletal muscle blood flow in healthy people and individuals at risk for or with heart failure*, Pro00040073 and *Cardiovascular Magnetic Resonance*, Pro00001460.

In this thesis a new method for the quantification and correction of the magnetic susceptibility effects of fat on the blood vessels contained within fat is proposed. There are four chapters in this thesis: Chapter 1 is the introduction that consists of a literature review and study motivation. Chapter 2 of this thesis contains the primary studies and findings on the measurement and correction for the magnetic susceptibility effects of fat in venous oximetry, and is being prepared for submission for publication in the *Magnetic Resonance in Medicine*. In Chapter 3, the application of our new methods for lower leg muscle oxygen consumption (VO_2) with plantar flexion exercise is illustrated. Chapter 4 contains the summary of the findings, the limitations of the study, and future directions.

Acknowledgements

I would first like to thank my supervisor, Dr. Richard Thompson, for accepting me as his student and for supporting and providing me extensive personal and professional guidance throughout my program. I really appreciate your care, motivation, and efforts to explain things clearly and simply. I could not have done it without your help.

I would like to thank my supervisory committee members, Dr. Alan Wilman and Dr. Atiyah Yahya for their insightful comments, encouragement, and hard questions from various perspectives. I appreciate your valuable comments on this thesis.

I would like to thank our group members, Joseph Pagano, Justin Grenier, Amy Kirkham, and Lingyu Xu for many scans, helpful suggestions and assistance with coding. Thank you for being part of my journey to make this thesis possible. Thank you to all the volunteers for your contribution and time.

Financial support for this thesis project was provided by the Canadian Institutes of Health Research (CIHR) and the Department of Biomedical Engineering, the Faculty of Medicine and Dentistry at the University of Alberta. Thank you to the Faculty of Graduate Studies and Research and the Graduate Students' Association for travel funding.

Finally, I would like to thank my family for their love, support, and prayers.

Table of Contents

Chapter 1: Introduction

Chapter 2: Measurement and Correction of the Bulk Magnetic Susceptibly Effects of Fat in MR Susceptometry of the Venous Blood Pool

2.3 Results

Chapter 3: Quantification of Muscle Oxygen Consumption (VO_2) with Dynamic Exercise

3.2 Methods

Chapter 4: Conclusions and Future Directions

List of Figures and Tables

List of Abbreviations and Symbols

3D	Three-dimension
ATP	Adenosine triphosphate
B_0	Main magnetic field strength
BF	Blood flow
BOLD	Blood oxygen level dependent
Ca	Oxygen carrying capacity
χ	Magnetic susceptibility
ΔB	Change in main magnetic field
$\Delta\chi$	Difference in magnetic susceptibility
$\Delta\chi_{do}$	Susceptibility difference between oxygenated and deoxygenated blood
ΔHbO_2	Deoxyhemoglobin
$\Delta\phi$	Difference in phase
ΔTE	Echo-time spacing
γ	Gyromagnetic ratio
$\gamma(^1H)$	Gyromagnetic ratio for a proton
GRE	Gradient-echo
HbO_2	Oxyhemoglobin
Hct	Hematocrit
Hb	Hemoglobin
MR	Magnetic resonance
MRI	Magnetic Resonance Imaging
O_2	Oxygen
PC	Phase contrast
PC-MRI	Phase-contrast magnetic resonance imaging
PET	Positron emission tomography
RF	Radio frequency
ROI	Region of interest
SaO_2	Arterial oxygen saturation
SvO_2	Venous oxygen saturation
T	Tesla, unit of magnetic field strength
T2	Transverse, spin-spin relaxation time
T2*	Effective transverse relaxation decay
TE	Echo time
θ	Angle between the vessel of interest and B_0
TRUST	T2 relaxation under spin tagging
v	Velocity of blood flow in phase contrast
VENC	Encoding velocity
VO_2	Oxygen consumption
VO_{2max}	Maximal whole body oxygen consumption
$VO_{2muscle}$	Oxygen consumption in working muscle

Chapter 1: Introduction

1.1 Introduction and Background

Exercise capacity, measured most commonly as the volume of oxygen consumed per time per kg of body mass (VO_2, ml/kg/min), is a major determinant of quality of life and survival in those with cardiovascular and a host of other diseases such as diabetes, obesity, cancer and liver disease (1,2). The vast majority of oxygen is consumed at the level of the exercising skeletal muscle. Skeletal muscle is the largest organ in the body, constituting 40-50% of total body mass in healthy individuals (3). Under various physiological challenges, the body maintains sufficient oxygen delivery and consumption based on demand (4,5). During exercise, skeletal muscle requires increased oxygen delivery to meet the increased metabolism of muscle contraction. The amount of oxygen delivered is dependent on the tissue metabolic requirement and on several physiologic parameters such as the arterial oxygen content, blood flow and hematocrit (Hct) (6-8). The difference in oxygen content between the afferent arterial blood and the efferent venous blood, and the amount of blood flow, together determine the amount of oxygen utilized by the tissue for its metabolic processes. Therefore, skeletal muscle oxygen consumption, $VO_{2muscle}$, can be estimated using knowledge of arterial and venous oxygen saturation and blood flow (either arterial or venous blood flow, which are equal). The normal arterial oxygen saturation, SaO_2, values are 97% to 99% in the healthy individual (9). In most studies, SaO_2 is assumed to be 98% for normal healthy individuals under resting conditions and mild exercise where arterial blood is almost fully oxygenated (9). Alternatively, SaO_2 can be measured using the finger pulse oximeter, which is routinely used for patient monitoring. Measurement of venous oxygen saturation, SvO_2 and venous blood flow will be described later in this chapter.

Traditionally, expired gas analysis during exercise is used to measure the whole body maximal oxygen consumption, VO_{2max}, which reflects the integrated aerobic fitness of an individual. However, this whole body VO_{2max} test does not provide a local measure of skeletal muscle oxygen consumption, nor does it distinguish the relative contributions of blood flow oxygen extraction to VO_2. In order to isolate the effects of skeletal muscle on limitations to whole body oxygen consumption, it is necessary to perform isolated muscle exercise. This will remove the potential limitations of the heart and larger conduit blood vessels on delivery of blood and oxygen to the muscle.

Monitoring of oxygen saturation in venous blood from the particular muscle group of interest provides a whole muscle assessment of the oxygen delivery and oxygen consumption in that muscle group. Therefore, robust and reliable methods to quantify venous oxygen saturation and venous blood flow, which determine the resulting muscle oxygen consumption in the exercising muscle, are needed to measure local physiological responses and to understand whether cardiac output (cardiac dysfunction) or local oxygen delivery and extraction (skeletal muscle dysfunction) is the limiting factor in exercise performance. Furthermore, local assessment of both oxygen extraction and blood flow will allow these two contribution factors to oxygen consumption to be evaluated independently.

1.2 Metabolism – Utilization of Oxygen in Exercising Muscle

Skeletal muscles need energy that is derived from adenosine triphosphate (ATP) to produce muscle contraction. Muscles tend to contain only limited quantities of ATP in the mitochondria. Thus, the rate of ATP hydrolysis (i.e. release of energy contained in ATP for muscle contraction) must be balanced by an equivalent rate of ATP synthesis to maintain ATP levels relatively constant so that the exercise can be continued (10). ATP production for muscle contraction occurs via phosphorylation within the cytosol at the level of creatine phosphate (PCr) breakdown (Figure 1.1a) and anaerobic glycolysis (Figure 1.1b) and via oxidative phosphorylation within mitochondria (Figure 1.1c).

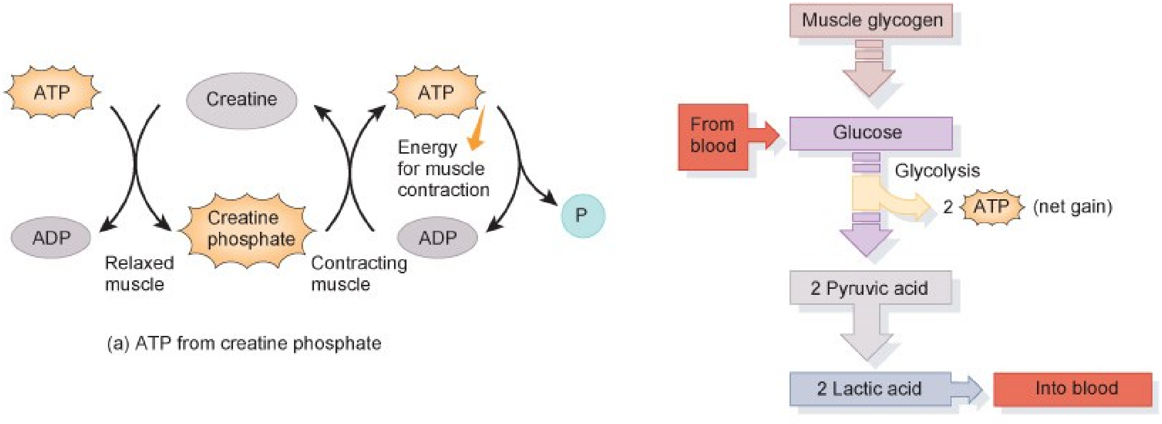

(a) ATP from creatine phosphate

(b) ATP from anaerobic glycolysis

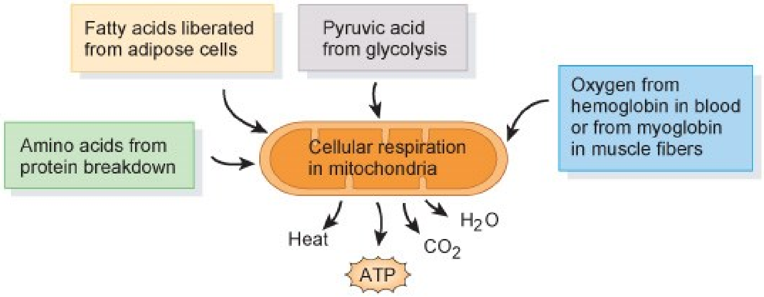

(c) ATP from aerobic cellular respiration

Figure 1.1 - ATP production for muscle contraction. Image from Introduction to the human body: the essentials of anatomy and physiology (11).

Different modes of ATP production are utilized based upon the exercise intensity and duration (12). However, training, diet and environmental conditions can also modify the metabolic response to exercise.

Oxygen plays an important role in both the aerobic and anaerobic metabolic systems. Aerobic metabolism fuels most of the energy needed for prolonged submaximal exercise. The

Citric Acid Cycle (CAC), a series of chemical reactions that use oxygen to convert energy sources including carbohydrates, fats, and proteins to carbon dioxide and ATP, is an aerobic process. Most cellular metabolism uses the aerobic metabolism system due to its high efficiency, as it generates 36 ATP per glucose. On the other hand, anaerobic metabolism occurs when the oxygen need for energy exceeds the oxygen supply. Anaerobic metabolism can only generate 2 ATP from one glucose molecule, and thus it provides energy during high intensity exercise of short duration. During anaerobic metabolism, creatine phosphate (CP) degradation to creatine (Figure 1.1a) and the breakdown of muscle glycogen to lactic acids (Figure 1.1b) are the major energy yielding pathways (13). However, the accumulation of lactic acid in muscle tissue and the lack of resources under conditions of high energy demand lead to muscle fatigue and muscle contraction stops (14). Oxygen is essential in the aerobic metabolism system to function, but it is also required in the anaerobic system to convert excess lactic acid back to glucose in the liver.

1.3 Invasive Methods to Measure Oxygen Consumption

In 1945, Kety and Schmidt described a method of measuring cerebral blood flow, cerebral metabolic rate and flux in humans based on the Fick principle. They used nitrous oxide or Kr^{85}, a metabolically inert and highly lipid-soluble gas, as the tracer of blood flow (15). The Fick principle states that the amount of a gas taken up or eliminated by a tissue per unit of time, Q(t), is equal to the difference between the amount in the entering arterial blood, $C_A(t)$ and the amount in the leaving venous blood, $C_V(t)$. Thus, the average cerebral blood flow per gram weight of brain is then:

$$\mathrm{CBF} = \frac{Q(t)/W}{\int (C_A(t) - C_V(t))dt} \qquad \text{Eq. 1.1}$$

where Q(t) is the amount of the inert gas taken up by the brain in time, t, and W is the brain weight (g), and $C_A(t)$ is the gas concentration in the arterial blood and $C_V(t)$ is the gas concentration in the venous blood.

Based on this fundamental principle, radioactive tracer clearance techniques were introduced. The radioisotope techniques measure blood flow by administering an inert radioisotope, ^{133}Xe and monitoring the exponential pattern of clearance of the radioisotope from the brain using sensitive detectors. Similarly jugular vein oximetry involves intravenous catheterization of a fiber optic probe and measuring oxygen delivery and oxygen extraction from the absorption spectrum of different wavelengths of light through optical measurements or Doppler ultrasound (16).

The blood flow and oxygen extraction can be measured, which in turn can be used to estimate the metabolic rate of oxygen consumption. However, invasive techniques have significant disadvantages including discomfort due to the catheterization, risk of infections, long data acquisition, and low temporal resolution (17). There are several non-invasive methods to measure oxygen consumption, which are summarized below.

1.4 Non-invasive Methods to Measure Oxygen Consumption

1.4.1 Positron Emission Tomography (PET)

In Positron Emission Tomography (PET), a very small amount of labelled radiotracer is either injected into the body, swallowed or inhaled as a gas and accumulates in the organ. The concentration of radiotracer in the tissue is measured by the imaging device.

Tissue oxygen extraction and metabolism can be measured by imaging the accumulated inhaled ^{15}O-labeled radiotracers in the tissue, where it is converted into ^{15}O-labeled water of metabolism (18-21). PET also uses intravenous injection of $H_2{}^{15}O$ water to quantify the blood flow. However, PET may not be preferable for exercise imaging due to several factors: restrictive positions, long scan times, and comparatively low spatial resolution (18,22). Also, PET imaging systems are relatively uncommon, requiring facilities to generate the isotopes on site, particularly for ^{15}O, which has a very short half-life of 122.24 seconds and complex system for constant delivery of the radiotracers.

1.4.2 Near-Infrared Spectroscopy (NIRS)

Near-infrared Spectroscopy (NIRS) is a non-invasive method for monitoring *in vivo* tissue oxygen availability and utilization (23-25). NIRS technique is based on measuring the attenuation of the near-infrared light (700-1000 nm wavelength) by the oxyhemoglobin and deoxyhemoglobin and cytochrome oxidase present in the tissue. The amount of light reflected after penetrating the tissue depends on the degree of scattering and the amount of absorption within the tissue.

NIRS is most commonly used due to its portability. NIRS is also relatively inexpensive, has excellent temporal resolution and relatively low noise amplitudes during movement like exercise. However, the spatial resolution of NIRS is low, the localization of the reflected signal is uncertain and NIRS methods cannot differentiate the signal of the arterial and venous blood (26-28). NIRS is also limited to superficial investigation due to the poor signal-to-noise ratio and the low intensity of penetrated light to deep tissue locations, with difficulty in individuals with substantial subcutaneous fat.

1.5 Magnetic Resonance Imaging (MRI)

Magnetic Resonance Imaging (MRI) measures oxygen saturation in venous blood with different techniques; either magnetization relaxation based techniques (29-32) or susceptometry based techniques (27,33-35).

Magnetic susceptibility, χ is a physical quantity that characterizes the magnetic response of a substance when placed in an external magnetic field. This can be expressed by:

$$\chi = \frac{J}{B0} \qquad \text{Eq. 1.2}$$

where J is the magnitude of the internal polarization and B_0 is the strength of the external field (Figure 1.2). The value of χ is given in ppm (parts per million). The magnetic induction within the material can be expressed as:

$$B = \mu_0(1+ \chi)H, \qquad \text{Eq. 1.3}$$

where B is units of Tesla, μ_0 is the permeability of free space and H is the magnetic field strength in ampere/meter. Susceptibility differences between tissues will create field inhomogeneities in uniform external fields, and can cause image distortions and loss of signal in MR images (36). However, local variations in susceptibility can be used to diagnose pathology or provide important information about tissue structure and function in the body (37).

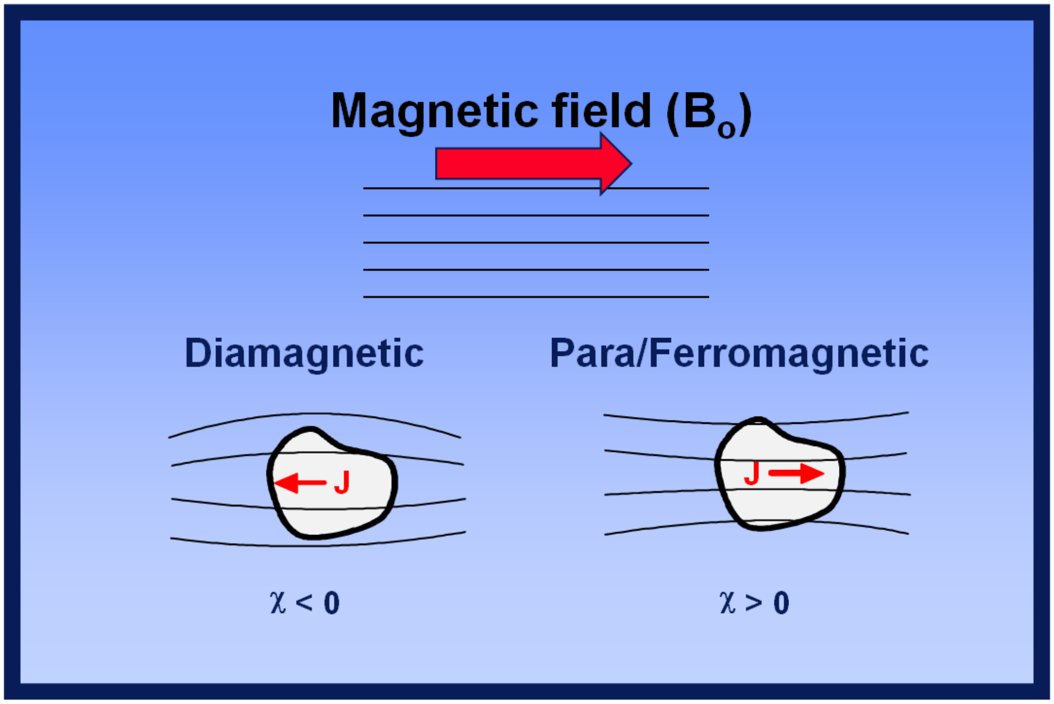

Figure 1.2 - Magnetic Susceptibility. When matter interacts with the magnetic field, an internal magnetization (J) is created that either opposes or is in the same direction as the external field. Courtesy of Allen D. Elster, MRIquestions.com

Based on the macroscopic behavior under the influence of an external magnetic field, various materials are classified into diamagnetic, paramagnetic, or ferromagnetic (36). If the susceptibility χ is negative ($\chi<0$), the material is considered as diamagnetic. If χ is positive ($\chi>0$), the material is paramagnetic. In the ferromagnetic case, $\chi>>0$. Almost all soft tissues in the body are diamagnetic in nature.

MRI is intrinsically sensitive to blood oxygenation based on the paramagnetic effects of deoxyhemoglobin. Hemoglobin, Hb, is the primary oxygen carrier in the red blood cell and is composed of four protein oxygen-carrying subunits, two alpha chains and two beta chains. Each protein subunit contains a heme molecule that consists of an iron atom (Fe^{2+}). In oxyhemoglobin (HbO_2), the iron atom is bound to oxygen with no unpaired electrons (Figure 1.3). HbO_2 exhibits diamagnetism, and thus is magnetically indistinguishable from surrounding tissues. Conversely, deoxyhemoglobin, $dHbO_2$ has four unpaired electrons that are exposed as the oxygen dissociates from the iron atom, with a significant magnetic moment. Thus, $dHbO_2$ is paramagnetic relative to the surrounding tissue (38).

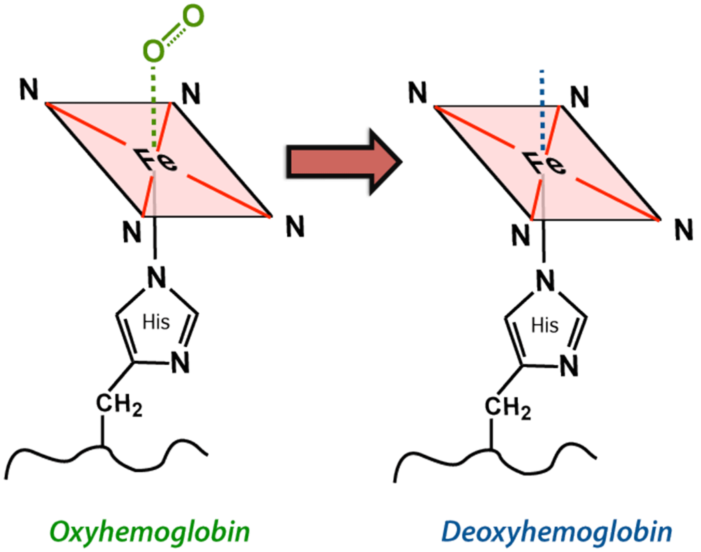

Figure 1.3 - Oxyhemoglobin and Deoxyhemoglobin. Deoxyhemoglobin is strongly paramagnetic due to four unpaired electrons at each iron center. Courtesy of Allen D. Elster, MRIquestions.com

1.5.1 Relaxation based techniques

Relaxation based techniques can measure blood volume and oxygenation based on the blood oxygen level dependent (BOLD) effect. T2 methods quantify intravascular transverse relaxation of blood caused by blood water protons diffusing through the magnetic field inhomogeneities. Such field inhomogeneities are created as a result of the frequency shifts between intra-and extra-erythrocyte spaces due to the paramagnetism of deoxygenated hemoglobin (39). Thus, the signal attenuation by T2 relaxation is enhanced as the concentration of deoxyhemoglobin increases. However, T2 methods have significant limitations including poor spatial resolution, low signal-to-noise ratio and image distortion by long acquisition times and motion, and sensitivity to partial volume effects from surrounding tissues (32,40-42). In order to convert the measured T2 to venous oxygen saturation levels, an ex-vivo calibration curve relating T2 and SvO_2 at different hematocrit and oxygenation levels needs to be measured using a blood perfusion phantom (32,43-45).

T2-Relaxation-Under-Spin-Tagging (TRUST) method measures T2 in the venous blood by applying spin tagging, similar to pulsed arterial spin-labelling (29,30,46,47). This method labels blood on the venous side of circulation and performs paired image subtractions. This allows the subtracted image to contain only venous blood signal and determine the T2 relaxation time of this signal and this T2 can be converted to venous oxygen saturation with a calibration curve. While TRUST has good reliability (48) and high SNR due to the large blood volume, measurements are restricted to terminal veins (49) and temporal resolution is low (50). The effects of inversion times also have to be accounted for and because it is a subtractive technique, it relies on negligible motion to ensure subtraction of unwanted background signals.

1.5.2 Magnetic Resonance Susceptometry-Based Oximetry

MR susceptometry-based oximetry is based on the measurement of the susceptibility difference, $\Delta\chi=\Delta\chi_{do}*Hct*(1-SvO_2)$ between the blood in the vein and its surroundings, where $\Delta\chi_{do}= 4\pi*0.27$ ppm (51) is the susceptibility difference (in SI units) between fully deoxygenated and fully oxygenated blood (33,34). Hematocrit, Hct is the fractional volume of red blood cells of the total volume of blood. The magnetic susceptibility of most tissues is very close to that of water (52), the predominant component of tissue. Therefore, muscle tissue serves as a magnetic field reference, relative to which the field of the venous blood signal can be measured (53).

In the magnetic field of an MRI scanner, susceptibility differences between the venous blood and the reference tissue result in frequency shifts. These shifts are due to the variation in the local magnetic field that causes the spins to precess at different frequencies. This results in phase differences that can be routinely measured using multi-echo gradient-recalled echo (GRE) acquisitions. Images with multiple echo-times (TEs) enable the measurement of phase-differences between images, $\Delta\varphi$. The local field shift, ΔB can be obtained for each pixel of the image from the phase difference:

$$\Delta\varphi = \gamma\Delta B\Delta TE \text{ and thus } \Delta B = \frac{\Delta\varphi}{\gamma * \Delta TE} \qquad \text{Eq. 1.4}$$

where $\Delta\varphi$ is the phase difference between multiple gradient-echoes separated by ΔTE and γ is the gyromagnetic ratio for a ^{1}H proton (γ=267.513 rad/sT). The relationship between the ΔB and $\Delta\chi$ can be described as:

$$\Delta B = d * \Delta\chi \qquad \text{Eq. 1.5}$$

where d is the dipole kernel and * is the process of convolution. Figure 1.4 below shows a two-dimensional cut of the three-dimension dipole kernel, showing the characteristic dipole-pattern.

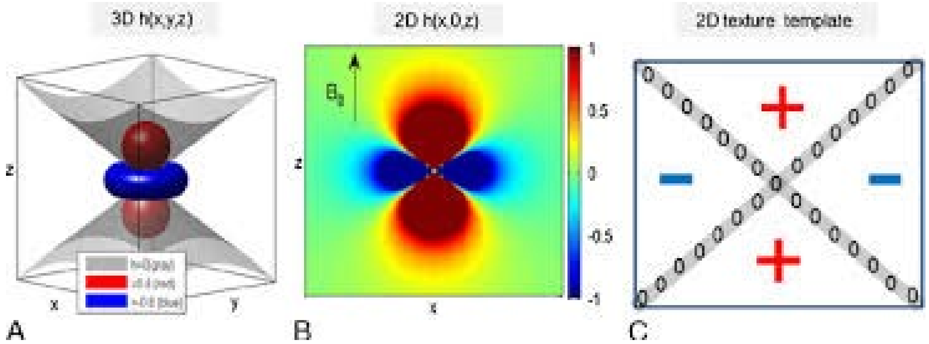

Figure 1.4 – The characteristic dipole-pattern.

In susceptometry methods, the blood vessel is modeled as a long paramagnetic cylinder (length >> diameter) (34) immersed in an external uniform magnetic field. For this situation, for a given susceptibility shift ($\Delta\chi$), the induced magnetic field (ΔB) inside the cylinder, relative to surrounding tissue can be approximated (34) as:

$$\Delta B = \frac{1}{6}\Delta\chi B_0(3\cos^2\theta-1) = \frac{1}{6}\Delta\chi_{do}*Hct*(1-SvO_2)\,B_0(3\cos^2\theta-1) \qquad \text{Eq. 1.6}$$

where θ is the vessel angle relative to the main magnetic field (B_0). The characteristic ($3\cos^2\theta-1$) term is the result of convolution of the dipole kernel, shown in Figure 1.4, and an infinite cylinder with a relative shift in magnetic susceptibility, $\Delta\chi$, relative to the surrounding material. By combining equation 1.4 and 1.6, the venous oxygen saturation can be calculated as:

$$SvO_2\,(\%) = 100 * \{1-\frac{2*\Delta\varphi/\Delta TE}{\gamma*\Delta\chi_{do}*Hct*B_0*(\cos^2\theta-1/3)}\} \qquad \text{Eq. 1.7}$$

The major strength of MR susceptometry-based methods are their robustness, acquisition speed, self-calibration and good temporal and spatial resolution, which are a result of the simple and efficient multi-echo gradient-echo acquisitions (53). These features make this approach preferable for imaging the oxygen saturation in venous blood with exercise challenges. In particular, the high blood velocities (rapid and complex motion) associated with exercise make the alternate T_2-based methods incompatible with exercise imaging.

Measurement of Blood Flow

The most widely used MRI technique to measure blood flow is the phase contrast (PC-MRI) method (54-56). PC-MRI method can be readily combined with the multi-echo gradient-echo field mapping methods to enable joint measurement of blood flow and oxygen saturation, which together can be used to estimate oxygen consumption.

1.5.3 Phase Contrast MRI

Phase contrast magnetic resonance imaging (PC-MRI) can quantify blood flow using velocity induced phase shifts. Typically, a bipolar gradient is used to encode velocity to image phase after excitation by a radio-frequency (RF) pulse. The stationary spins experience no net phase shift in relation to motion, but the moving spins will acquire a net phase shift as they move along the direction of a magnetic field gradient (57,58). In the phase difference image, the signal phase is linearly proportional to the velocity of the spins in each pixel; faster moving spins in one direction give rise to a higher positive phase, whereas blood moving in the opposite direction is assigned higher negative phase. Thus, the speed and direction of the blood flow can be quantified.

Due to the cyclic nature of image phase ($-\pi$ to π), phase contrast imaging is usually only applied over a range of velocities that correspond to this range of phases. To specify this range of velocities, a velocity-encoding (VENC) value can be chosen by a user. It determines the highest and lowest detectable velocity encoded by a phase-contrast sequence. The VENC parameter corresponds to the velocity that will give rise to phase shifts of $\pm\pi$. VENC is usually given in centimeters per second.

The signal in each pixel in a phase difference image is linearly proportional to the velocity of the blood by that pixel. Velocity in pixel can be expressed as:

$$v = \text{VENC} * (\text{pixel phase difference} / \pi) \qquad \text{Eq. 1.8}$$

and labelled with direction. A region of interest (ROI) can be drawn on the image to measure the velocity of the blood directly. In addition, flow volumes can be calculated from the equation:

$$Q = v * A \qquad \text{Eq. 1.9}$$

where Q is flow in mL/min, v is the average velocity (cm/sec) of all pixels in the region of interest (ROI), which is determined by using the phase images and A is the area of the vessel (cm^2) which is defined by a user-generated ROI.

PC-MRI provides flexibility of image spatial and temporal resolution to suit the application and can be repeated for all directions of flow at any location in the body (59). However, in order to account for non-velocity image phase, from off-resonance frequencies, two images must be acquired, with different bipolar gradient pairs but with identical echo-times. Phase-difference processing removes the off-resonance image phase, and the different bipolar gradients define the flow-encoding strength, or VENC, for the acquisition.

1.6 Exercise in the MRI

1.6.1 Target Muscles and Vein of Interest

The ultimate goal of the work to be enabled by this thesis is to measure the skeletal muscle oxygen consumption in an isolated muscle with exercise. Isolated exercise has the potential to expose muscle-specific limitation to exercise capacity (blood flow to that muscle and oxygen extraction in that muscle) as opposed to conventional whole body exercise, in which several factors act in unison to reduced exercise capacity, which are difficult to untangle (e.g. lung function, heart function, vascular function at many locations).

In order to study isolated muscle with exercise the muscle group should be a well-defined functional group, exercisable in isolation and with direct blood flow to and from the muscle group (60). The gastrocnemius muscle which is targeted with plantar-flexion exercise was used for our study. The blood oxygen saturation and blood flow in the popliteal vein (Figure 1.5) were measured to estimate the whole lower leg muscle oxygen consumption at rest and with exercise.

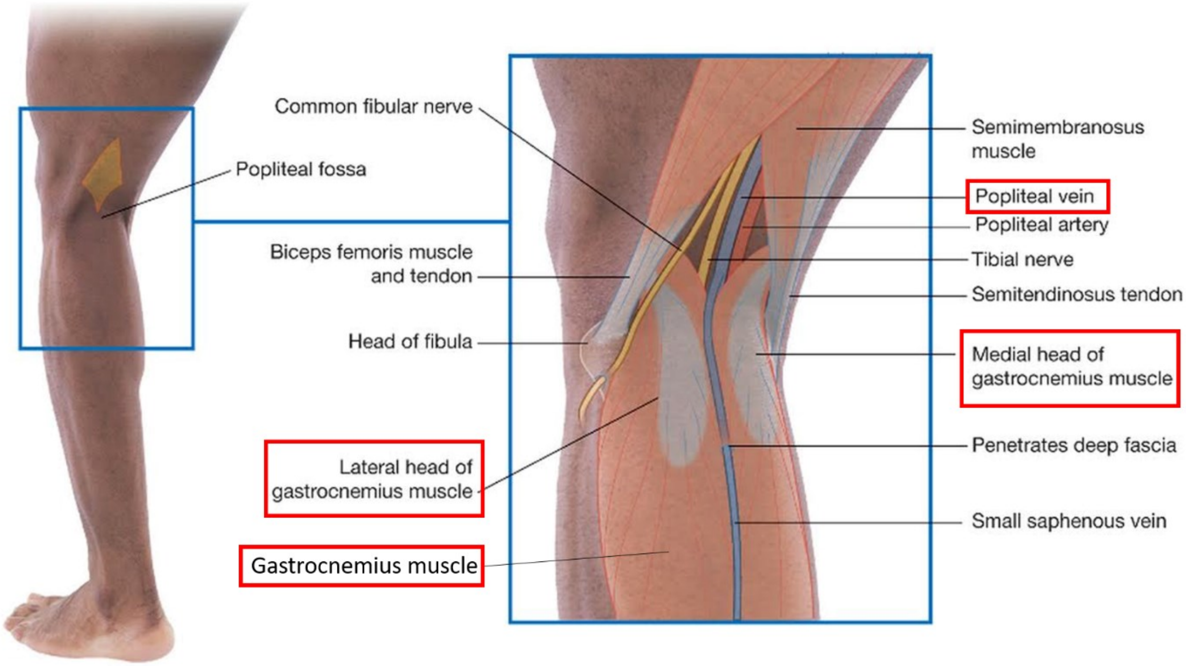

Figure 1.5 - Visualizing the contents of the popliteal fossa. Image from Gray's basic anatomy (61).

1.6.2 Oxygen Consumption

The skeletal muscle oxygen consumption, $VO_{2muscle}$, can be estimated by combining arterial and venous oxygen saturation and venous blood flow measurements using Fick's principle (15).

$$VO_{2Muscle} = Ca * VBF * (SaO_2 - SvO_2) \qquad \text{Eq. 2.0}$$

where Ca is the oxygen carrying capacity of hemoglobin, VBF is the total venous blood flow to the muscle, SaO_2 and SvO_2 represent the arterial and venous oxygen saturation levels, respectively. Ca = 1.34 mL O_2/g Hb, and hemoglobin is commonly assumed to have a concentration of 14.6 g/dL (at the Hct of 0.43). At rest, the normal range of SvO_2 is 50-75% (62), and the normal values for SaO_2 are in the range of 97-99% (9,35). SvO_2 can be estimated by MR susceptometry and SaO_2

is measured with a pulse oximeter (inexpensive finger device). VBF is quantified with the phase-contrast MRI technique. By interleaving sequences for venous blood flow and venous saturation measurement, both parameters are simultaneously measured to assess whole lower leg muscle oxygen consumption. Imaging immediately post-exercise allows characterization of end-exercise peak values and oxygen recovery kinetics from peak exercise.

Oxygen recovery kinetics refer to the rate of change in VO_2 after exercise (63,64). VO_2 recovery time, τVO_2, is most commonly defined as the time-constant of exponential recovery. Slowed *whole body* VO_2 recovery kinetics, as compared to healthy subjects, is a well-established feature of heart failure patients (65,66). However, the muscle-specific contributions to delayed recovery is not well characterized, the study of which would be enabled by muscle-specific VO_2 tests. VO_2 recovery kinetics also have the advantage of being insensitive to exercise intensity (65). This has the advantage of improved test reproducibility by removing the direct dependence on participant effort. Measurements of the VO_2 and VO_2 recovery kinetics in an isolated muscle remove the potential limitations of heart function for oxygen delivery and provide information about the skeletal muscle function to the mechanisms reducing exercise capacity (67,68), which ultimately will enable a better understanding of the mechanisms of reduced exercise capacity.

1.7 Confounders to Susceptometry – Effects of Fat

1.7.1 Limits of Reference Tissue Region

In MR susceptometry-based oximetry, the relative susceptibility of blood in the vein with respect to surrounding reference tissue is used to quantify venous oxygen saturation. The magnetic susceptibility of venous blood depends linearly on the volume fraction of the paramagnetic deoxyhemoglobin in red blood cells (53). However, we do not directly measure magnetic susceptibility, rather, we measure the magnetic field perturbation caused by the differences in magnetic susceptibility between deoxygenated blood and reference tissues surrounding the vein. Most body tissues have magnetic susceptibilities close to that of water (52), therefore the surrounding muscle tissues can be used as a reference with known susceptibility. Unfortunately, the conduit veins in the periphery that return blood from the calf and quadriceps muscles are often surrounded by fat. Fat surrounding the conduit veins limits the region of the reference (muscle) tissue as indicated in Figure 1.6. The fat also may directly affect the local magnetic field distribution as a consequence of its distinct magnetic susceptibility, further exacerbating the process of estimation of the field shift by deoxyhemoglobin alone. The magnetic field environment of fat is reviewed in the following section.

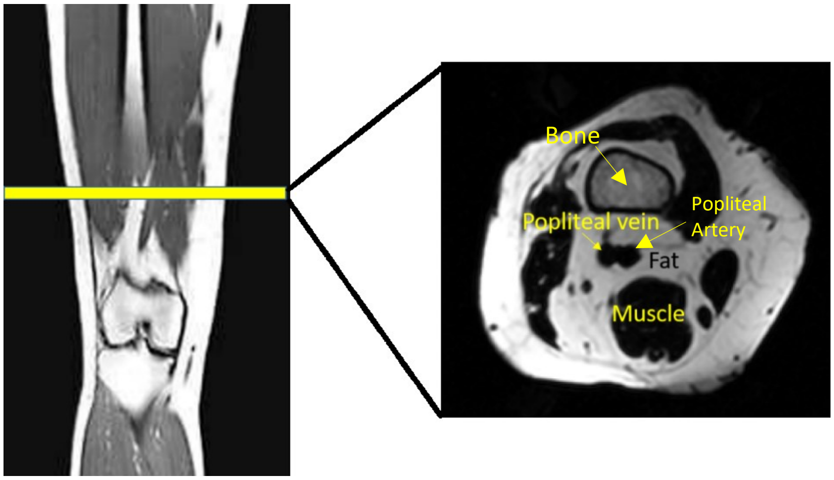

Figure 1.6 - Fat surrounding the popliteal vein and regions of muscle tissues. All the dark regions within the fat are muscle except the vein and artery.

1.7.2 Magnetic Susceptibility and Chemical Shift of Fat

The chemical environment of a proton in water (H_2O) is different than a proton in fat (CH_2). The electron clouds surrounding the proton (i.e. ^1H) shields it from the applied external field, where the electronic shielding of the protons in the fat molecules is greater than protons in water molecules. More shielded protons in fat experience a smaller effective magnetic field, and thus resonate slightly slower than water protons, with a shift that is proportion to the applied static magnetic field, B_0.

For example, at 3T, the resonance frequency of ^1H is approximately 128 MHz according to Larmor equation:

$$\omega = \gamma * B_0 \qquad \text{Eq. 2.1}$$

where ω is the frequency of precession, γ is the gyromagnetic ratio (42.58 MHz/T for the ^1H nucleus), and B_0 is the strength of the applied external field. The chemical shift between fat and water is approximately 3.5 ppm when water is taken as reference. Thus, fat-water frequency difference, Δf would be:

$$\Delta f = (128*10^6\ \text{Hz})*(3.5*10^{-6}) = 440\ \text{Hz}. \qquad \text{Eq. 2.2}$$

Because fat contains several protons in distinct chemical environments, it has a characteristic spectrum of chemical shifts, typically [-3.73, -3.33, -2.53, -1.87, -0.32, 0.67] ppm relative to water with normalized amplitudes [0.087, 0.693, 0.128, 0.004, 0.039, 0.048] (69).

While chemical shift refers to the effects of the charge structure on the protons contained within them in response to an external magnetic field, the magnetic susceptibly refers to the effects of the charge structure on the environment outside of the electron clouds. Fat has a distinct magnetic susceptibility from the surrounding muscle tissue and the blood in the vein ($\chi_{Fat} = 0.65$ ppm as compared to water) (70), which may confound estimation of our targeted venous oxygen saturation, which is based on the local perturbation of the magnetic field arising from its distinct magnetic susceptibility.

1.8 Motivation of the Study

Whole body oxygen consumption, which is commonly measured using expired gas analysis (metabolic cart), reflects the aerobic physical fitness of an individual, but cannot distinguish the contributions of cardiac function, blood flow and oxygen extraction by the muscles in the study of reduced exercise capacity. Measurement of oxygen extraction and blood flow at the level of the skeletal muscle is very important for describing the physiological and pathological state of the skeletal muscle (53).

Magnetic susceptometry has been used for the non-invasive estimation of local venous oxygen saturation based on the magnetic susceptibility differences between the blood in the vein and its surrounding tissues (35,53,71,72). In order to quantify venous oxygen saturation accurately with this method, it is important to know the orientation of the vessel with respect to the main magnetic field and to have sufficient and suitable surrounding reference tissue. However, the conduit veins in the periphery are often surrounded by fat which itself has a different magnetic susceptibility than the surrounding reference water and the targeted venous blood pool (χ_{Fat}=0.65 ppm) (70,73). This magnetic susceptibility of fat might cause potentially complex variations in the static magnetic field in skeletal muscle. The resulting perturbation of the magnetic field by the fat, both within the vein and in surrounding reference muscle tissue is unknown and may confound measurement of the targeted shift in the local field by deoxyhemoglobin alone, and thus contaminate estimation of venous oxygen saturation.

In this thesis, we propose a novel method to measure and characterize the magnetic susceptibility effects of fat on venous oxygen saturation imaging and to correct for the confounding effects of the fat. We measure the angle between the vessel and the main magnetic field and correct for the effects of vessel orientation on SvO_2 measurement. The feasibility of this approach in the popliteal vein (venous return from the lower leg) in conjunction with plantar flexion (calf muscle) exercise was also evaluated.

Chapter 2: Measurement and Correction of the Bulk Magnetic Susceptibly Effects of Fat in MR Susceptometry of the Venous Blood Pool

2.1 Introduction

Venous oxygen saturation (SvO_2) reveals oxygen extraction and consumption from upstream organs, with applications for the study of metabolism in several tissues including the brain (33-35,74), skeletal muscle (60,75) and others (71,76,77). Magnetic susceptometry has been used for the non-invasive estimation of SvO_2, taking advantage of the linear relationship between the concentration of deoxyhemoglobin and magnetic susceptibility of blood, χ_{Blood} (71,76). For the case of cylindrical blood vessels, χ_{Blood} has an analytic relationship to the shift in the magnetic field within the vessel, which can be readily measured with MRI (53,72). However, it is common for conduit veins of interest, particularly in the periphery, to be surrounded by fat, which has a different magnetic susceptibility from the targeted venous blood pool and the surrounding reference water in nearby muscle tissue (70,73). The resulting perturbation of the magnetic field by the fat, both within the vein and in the surrounding reference tissue, may confound measurement of the targeted shift in the local field by deoxyhemoglobin alone, and thus contaminate estimation of SvO_2. Additionally, the large magnetic field shift within the fat pool precludes the use of the fat region itself as a reference tissue, for calculation of the relative shift within the vein.

The goals of the current study were to measure and characterize the magnetic susceptibility effects of fat on SvO_2 imaging and to develop a new method to correct for the confounding effects of the fat. The feasibility and reproducibility of this approach in the popliteal vein (venous return from the lower leg) at rest and with plantar flexion exercise was evaluated.

2.2 Methods

2.2.1 Imaging of Venous Oxygen Saturation (SvO_2): Current Methods

MRI susceptometry is used to estimate SvO_2 based on the well-characterized relationship between the magnetic susceptibility of blood (χ_{Blood}) and SvO_2, $\chi_{Blood}=\chi_{do}*Hct*(1-SvO_2)$, where $\chi_{do}=4\pi*0.27$ppm is for fully deoxygenated blood and Hct is hematocrit (33). For the case cylindrical vessels at an angle of θ to the main magnetic field (B_0), the venous oxygen saturation can be estimated from the shift in magnetic field within the vein (ΔB_{O2}) according to:

$$SvO_2(\%) = 100*[1-2*\Delta B_{O2}/(\gamma*\chi_{do}*Hct*B_0*(\cos^2\theta-1/3))] \qquad \text{Eq 2.1}$$

where γ is the ^{1}H gyromagnetic ratio ($\gamma = 42.576$MHz/T) (33,34). This approach has been used to image SvO_2 in the brain (33,34) and in skeletal muscle at rest (27,75), with arterial occlusion (27), and with exercise (60).

In order to measure the magnetic field shift arising from the concentration of deoxyhemaglobin alone, the effects of static magnetic field inhomogeneity need to be accounted for by estimation and subtraction of the background field, $\Delta B_{Background}$, which can be measured in reference tissue surrounding the vein of interest. In the periphery, skeletal muscle surrounding the vein of interest is used as a reference tissue that is assumed to have a uniform magnetic susceptibility that is approximately equal to fully oxygenated blood (27,72). Typically, a best-fit low spatial frequency evaluation of $\Delta B_{Background}$ in the muscle is used to estimate this field at the location of the vein, to enable subtraction of the unwanted $\Delta B_{Background}$ component (72). This standard approach is illustrated in Figure 2.1, showing subtraction of a best-fit field from the measured field for calculation of ΔB_{O2} in the popliteal vein of a volunteer, where $\Delta B_{O2} = \Delta B_{Measured} - \Delta B_{Background}$ within the vein. Note that the fat surrounding the vein in this example was excluded for the estimation of $\Delta B_{Background}$ due to large field shift from chemical shift and magnetic susceptibility effects of the fat, within the fat pool.

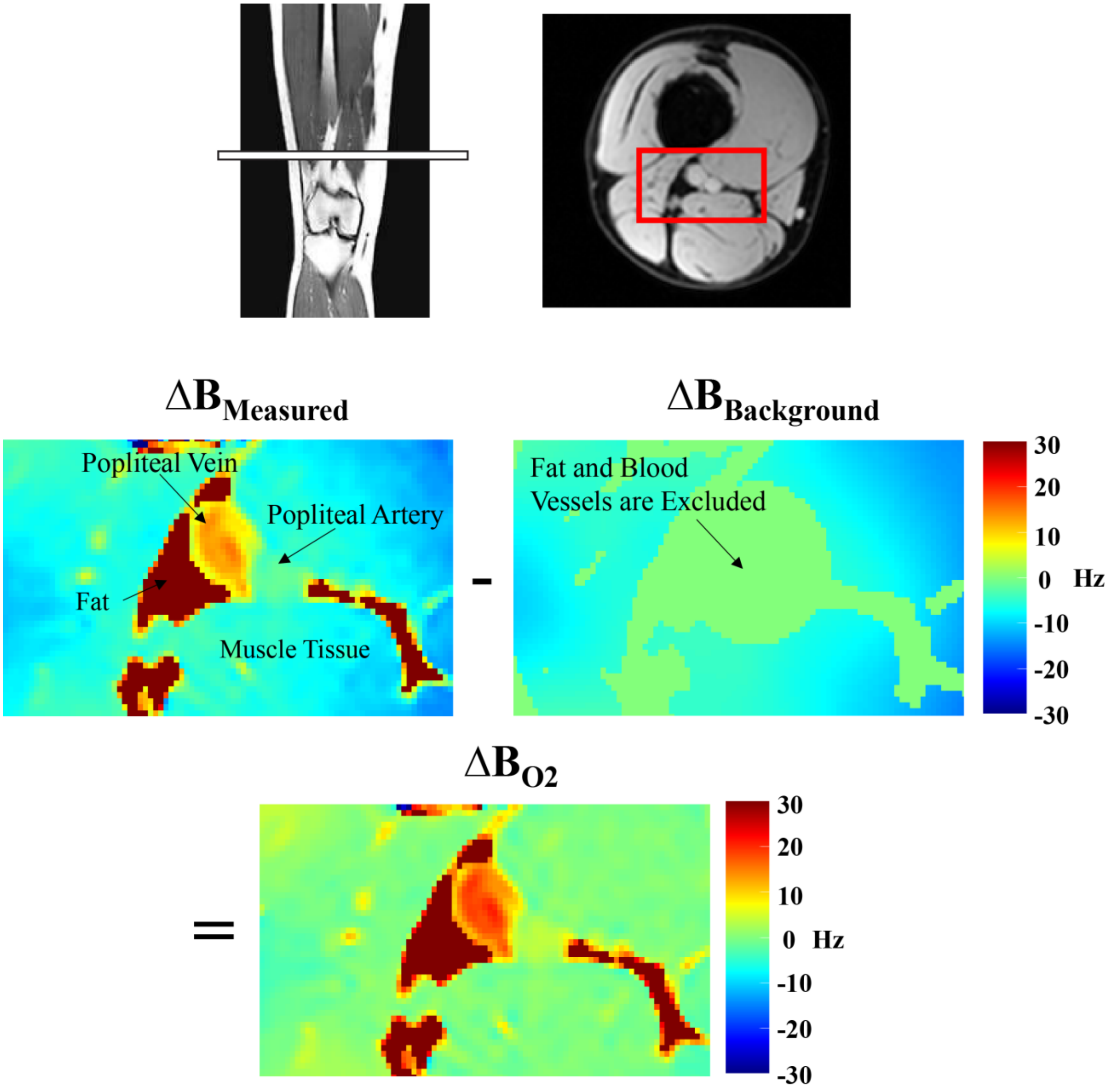

Figure 2.1 - Conventional background correction method. The background off-resonance field, $\Delta B_{Background}$, is measured in segmented muscle tissue regions, and interpolated to the full image prior to subtraction from the measured field, $\Delta B_{Measured}$. The resulting field map reflects on the field shift from deoxyhemoglobin in the vein, ΔB_{O2}, but with large residual off-resonance frequencies in the fat pool.

2.2.2 Measuring and Correcting the Effects of the Magnetic Susceptibility of Fat

The conduit veins of interest in the periphery, returning blood from the quadriceps muscle (femoral vein) or calf muscle (popliteal vein), for example, are commonly surrounded by fat, particularly where smaller veins converge to the larger targeted veins. The potentially complex magnetic field perturbations from the fat (ΔB_{Fat}), which are a consequence of its distinct magnetic susceptibility ($\chi_{Fat} = 0.65$ ppm as compared to water (70)) and complex geometry, will extend outside of the fat into the vein and the surrounding muscle reference tissue, which may confound estimation of the targeted ΔB_{O2} in the vein. Additionally, the fat region cannot be used to define the background field (Figure 2.1), which may limit the accuracy of the field estimation at the location of the vein, as a function of the thickness of the fat region surrounding the vein.

In the presence of fat, the resulting magnetic field within and surrounding the vein can be expressed as a sum of three components, $\Delta B_{Measured} = \Delta B_{O2} + \Delta B_{Background} + \Delta B_{Fat}$. ΔB_{Fat} has contributions from both magnetic susceptibility, $\Delta B_{Fat(\chi)}$, and from chemical shift (CS) effects, $\Delta B_{Fat} = \Delta B_{Fat(CS)} + \Delta B_{Fat(\chi)}$.

The conventional approach to measure the static magnetic field distribution, $\Delta B_{Measured}$, utilizes the phase difference between images acquired at incremented echo times, $\Delta B_{Measured} = (\phi_{(TE2)} - \phi_{(TE1)})/(TE_2 - TE_1)$, as shown in Figure 2.1 (78). In the current study, we propose to use a multi-echo gradient-echo Dixon fat-water separation method (69) to measure both the total static magnetic field, $\Delta B_{Measured}$, as well as the distribution of fat around the targeted vein, using the calculated fat and water separated images. This approach has the advantage of calculation and removal of chemical shift contribution of the fat, $\Delta B_{Fat(CS)}$, from the measured magnetic field as an intrinsic component of the least squares solution to fat and water separation and calculation of

$\Delta B_{Measured}$ (69,79). Additionally, the measured distribution of fat can subsequently be used to calculate the magnetic field perturbation, $\Delta B_{Fat(\chi)}$, based on the known magnetic susceptibility of fat (80,81). Finally, it is proposed that with correction for the chemical shift and magnetic susceptibility of fat, $\Delta B_{Fat(CS)} + \Delta B_{Fat(\chi)}$, that the background field calculation can include the normally excluded fat region.

Figure 2.2 outlines the proposed procedure for measurement and removal of ΔB_{Fat} and calculation of the targeted venous ΔB_{O2} field. The Dixon method provides fat and water separated images, and thus a direct calculation of fat-fraction images, which are used to generate the corresponding magnetic susceptibility images, $\chi_{(x,y,z)} = 0.65{*}FF_{(x,y,z)}$, from which $\Delta B_{Fat(\chi)}$ can be directly calculated (Figure 2.2, top row). The calculation of $\Delta B_{Fat(\chi)}$ will be described in 2.2.3. The Dixon method also provides a direct measure B_0 field map ($\Delta B_{Measured}$), which can be corrected using $\Delta B_{Fat(\chi)}$ prior to fitting the background field (Figure 2.2, middle row), $\Delta B_{Corr} = \Delta B_{Measured} - \Delta B_{Fat(\chi)}$. Finally, the background field can be measured using the fat-corrected images, similar to the conventional approach shown in Figure 2.1, however, with a larger reference region, including all fat and muscle tissue outside the artery and vein (Figure 2.2, bottom row).

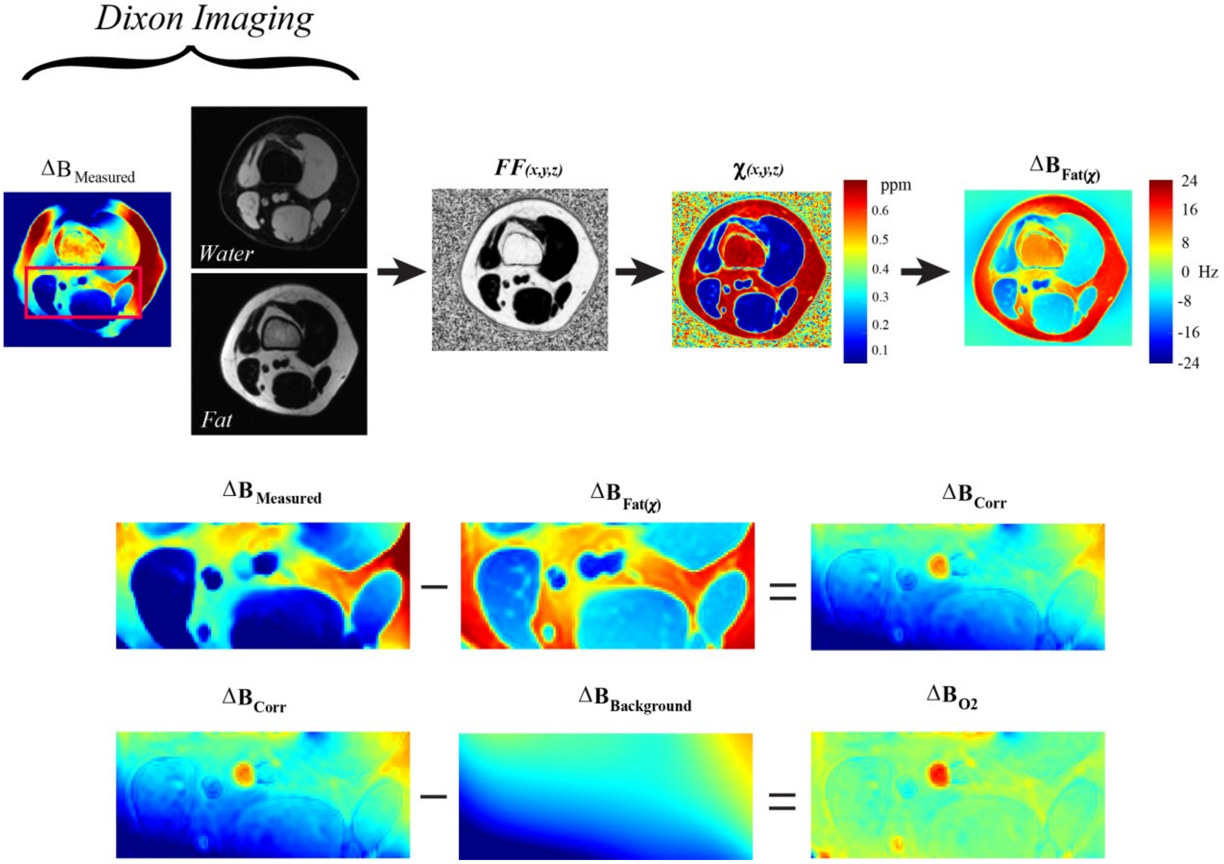

Figure 2.2 - Dixon fat-water separated imaging yields off-resonance, fat and water images. Fat fraction images (FF) are used to generate a susceptibly map based on fat content, $\chi_{(x,y,z)}$, which can be used to calculated the expected susceptibility-related off-resonance effects, $\Delta B_{Fat(\chi)}$ (**Top**). A corrected off-resonance image, ΔB_{Corr}, can be generated by subtraction of $\Delta B_{Fat(\chi)}$ (**Middle**). The background magnetic field, $\Delta B_{Background}$, can be measured from the corrected field, and subtracted to yield an off-resonance image in the targeted vein that is dependent only the magnetic susceptibility (oxygen saturation) of the vein, ΔB_{O2} (**Bottom**). One of 49 slices is shown.

Using this approach, our specific goals are: 1) to determine if ΔB_{Fat} has a significant effect on the measured magnetic field outside the fat region, within the popliteal vein and in the surrounding muscle tissue, 2) to evaluate the efficacy of the proposed method for removal of ΔB_{Fat},

3) compare the resulting ΔB_{O2} (SvO_2) values in a targeted slice with and without removal of ΔB_{Fat}, (i.e. comparison to the current standard approach) and 4) illustrate the compatibility of this approach with plantar-flexion exercise, to measure peak exercise values and recovery dynamics for SvO_2.

2.2.3 Evaluation of ΔB_{Fat}

The magnetic field shift associated with the magnetic susceptibility of fat, χ_{fat}, can be directly calculated using $\Delta B_{Fat} = F^{-1}[(1/3 - k_z^2/k^2)F\chi_{fat}]B_0$ where F and F^{-1} are the forward and inverse Fourier transforms; $k^2 = k_x^2+k_y^2+k_z^2$ and k_x, k_y, k_z are the k-space coordinates with k_x and k_y in plane and k_z along the B_0 direction (81). This approach requires the three-dimensional distribution of magnetic susceptibility as in input, $\chi_{(x,y,z)}$, even for the calculation of $\Delta B_{Fat(\chi)}$ in a single targeted slice. The sample data in Figure 2.2 is one slice from 49 slices used for the calculation of ΔB_{Fat}. The influence of the extent of spatial coverage (the number of slices) on the calculated field, $\Delta B_{Fat(\chi)}$, in a targeted central slice location (i.e. location for assessment of SvO_2) was evaluated as a function of the number slices in the input magnetic susceptibility data, $\chi_{(x,y,z)}$ (82).

2.2.4 Compatibility of SvO_2 Imaging with Dynamic Exercise Studies

Evaluation of SvO_2 in combination with exercise (60) or other interventions (27,34) requires sufficient temporal resolution, typically on the order of several seconds or less, to characterize peak values and changes over time (e.g. rate of recovery following exercise or venous occlusion). However, estimation of ΔB_{Fat} from susceptibility maps, $\chi_{(x,y,z)}$, will require three-dimensional acquisitions, demanding longer imaging times that are not compatible with dynamic time-resolved experiments. In the current study, we propose to use a separate multi-slice acquisition to calculate $\Delta B_{Fat(x,y,z)}$, which is used to correct dynamic single-slice acquisitions with sufficient temporal resolution to resolve dynamic events, to calculate the targeted $\Delta B_{O2}(t) = \Delta B_{Measured}(t) - \Delta B_{Background}(t) - \Delta B_{Fat}$. Registration (83) of the dynamic single slice images with static images used to calculate ΔB_{Fat} was used to ensure image alignment prior to correction.

2.2.5 Subjects

Ten healthy subjects (5 male and 5 female; 27 ± 3 yrs) provided written informed consent following an institutional review board-approved protocol.

2.2.6 Pulse sequence

All experiments were performed on a 3T MRI scanner (3T PRISMA; Siemens Healthcare; Erlangen, Germany). A slice interleaved multi-echo gradient-echo pulse sequence, with monopolar readout gradients, was used for three-dimensional Dixon imaging. Acquisition parameters were 49 slices with 4 mm slice thickness (no gap) with flow-compensation, 192 x 102 acquisition matrix, 280 x 149 mm field of view, 1445.00 Hz/pixel receiver bandwidth, TE= [2.44, 4.26, 6.08, 8.90, 9.72, 11.54] ms, TR = 14.29 ms ($TR_{effective}$ = 700 ms), flip angle = 30° and a 75 seconds total acquisition time. A flexible four-element surface coil was used for signal reception and the body coil was used for excitation. Magnitude and phase images were reconstructed.

A similar pulse sequence was used for post-exercise dynamic imaging, with identical TE values and receiver bandwidth. The slice prescription matched the central of 49 slices from the three-dimensional acquisition above. The flip angle was reduced to 20° and TR was increased to 18.9 ms due to inclusion of slice-selective saturation pulse every TR, applied parallel and superior to the imaging slice, to eliminate the pulsatile arterial blood pool signal (60). Sequential singleshot images were acquired in 102 k-space lines/image*18.9 ms/line = 1.93 seconds/image, with 50 repetitions.

Slice prescriptions targeted long straight sections of the popliteal vein that were approximately parallel to the B_0 field and superior to the knee, in order to capture venous return from the lower leg. To visualize the venous anatomy for slice prescription on the popliteal vein, an arterial saturation venogram was acquired with coverage from the knee to lower thigh: 30 slices, 2.5 mm slice thickness, 256 x 192 acquisition matrix, 280 x 210 mm, 150 Hz/pixel receiver bandwidth, TR/TE = 50 ms/5 ms, flip angle = 60°, with a gradient echo readout and a total scan time of 90 seconds.

2.2.7 Bloch Equation Simulations

Bloch equation simulations of the multi-slice multi-echo gradient-echo acquisition were used to calculate the signal yield as a function of T_1, to determine the relative water and fat signal yield, for potential T_1 correction of the fat fraction maps. Identical pulse sequence parameters including the distribution of flip angles from excitation slice profile were included in simulations. T_1 values of water and fat of 1400 ms and 370 ms (3T MRI scanner), respectively, were assumed (84).

2.2.8 Exercise Device and Protocol

An air pressure based ergometer (Trispect; Ergospect; Innsbruck, Austria) was used for plantar-flexion exercise, targeting the gastrocnemius muscle group in the calf. All subjects performed incremental exercise (4-9 Watts, increasing 1 Watt/minute) for 3-6 minutes with a goal of 75% of peak intensity. Post-exercise imaging started within 1 second of the completion of exercise, with acquisition repetition every 3.86 seconds, to capture end-exercise values and recovery dynamics.

2.2.9 Vessel Angle Measurement and Correction

The multi-slice multi-echo Dixon acquisition was used for identification of the popliteal vein in all 49 slices, for calculation of the orientation of the popliteal vein relative to the main magnetic field as a function of location. The center of the vein along its length was selected and used to define the angle of the vessel with respect to the main magnetic field.

2.3 Results

Bloch equation simulations of the multi-slice multi-echo acquisition yielded fat and water signal yield of 20.2% and 19.0%. To correct with small difference in signal yield, fat images were scale by 0.9406 prior to calculation of fat fraction map used to calculate fat susceptibility maps, for calculation of $\Delta B_{Fat.}$

2.3.1 Multi-Slice Acquisitions

Figure 2.3 shows the spatial coverage provided by the multi-slice multi-echo acquisition, with three sample slices (from 49 slices) displaying fat and water separated images and the corresponding calculated off-resonance maps, $\Delta B_{Measured}$. The typical orientation of the popliteal vein over this region, as measured with the arterial saturation venogram, is shown on the left.

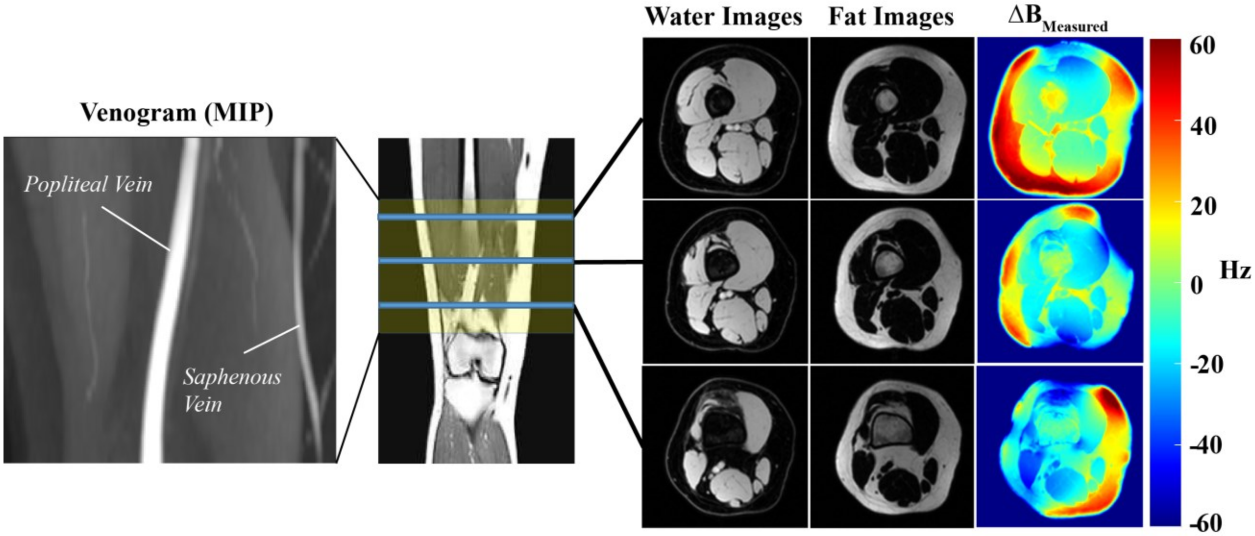

Figure 2.3 - Typical multi-slice multi-echo Dixon acquisition showing the extent of the spatial coverage on the lower thigh (49 slices, 4mm slice thickness, no gap). The orientation of the targeted popliteal vein in the lower thigh is shown on the left. The output of the Dixon processing for three sample slices, off-resonance, water and fat images, is shown on the right for three slices.

Calculation of the targeted magnetic field shift within the popliteal vein, with correction for the effects of fat and the background magnetic field, $\Delta B_{O2} = \Delta B_{Measured} - \Delta B_{Background} - \Delta B_{Fat}$, is illustrated in four sample slices in a different volunteer (Figure 2.4). The bottom panels compare the background field correction in slice 1 using only the muscle as a reference region (i.e. the conventional method) versus the full region surrounding the vein, following removal of the ΔB_{Fat} component, highlighting the differences in the calculated $\Delta B_{Background}$ fields. The effects of the background correction on the targeted magnetic field in the vein is illustrated in Figure 2.5. The conventional method (Figure 2.5C), while yielding a well corrected background in the muscle reference tissues, has significant errors in the artery and vein regions. Specifically, there is a large negative field shift in the artery and reduced shift in the vein as compared to the fat removal method (Figure 2.5B).

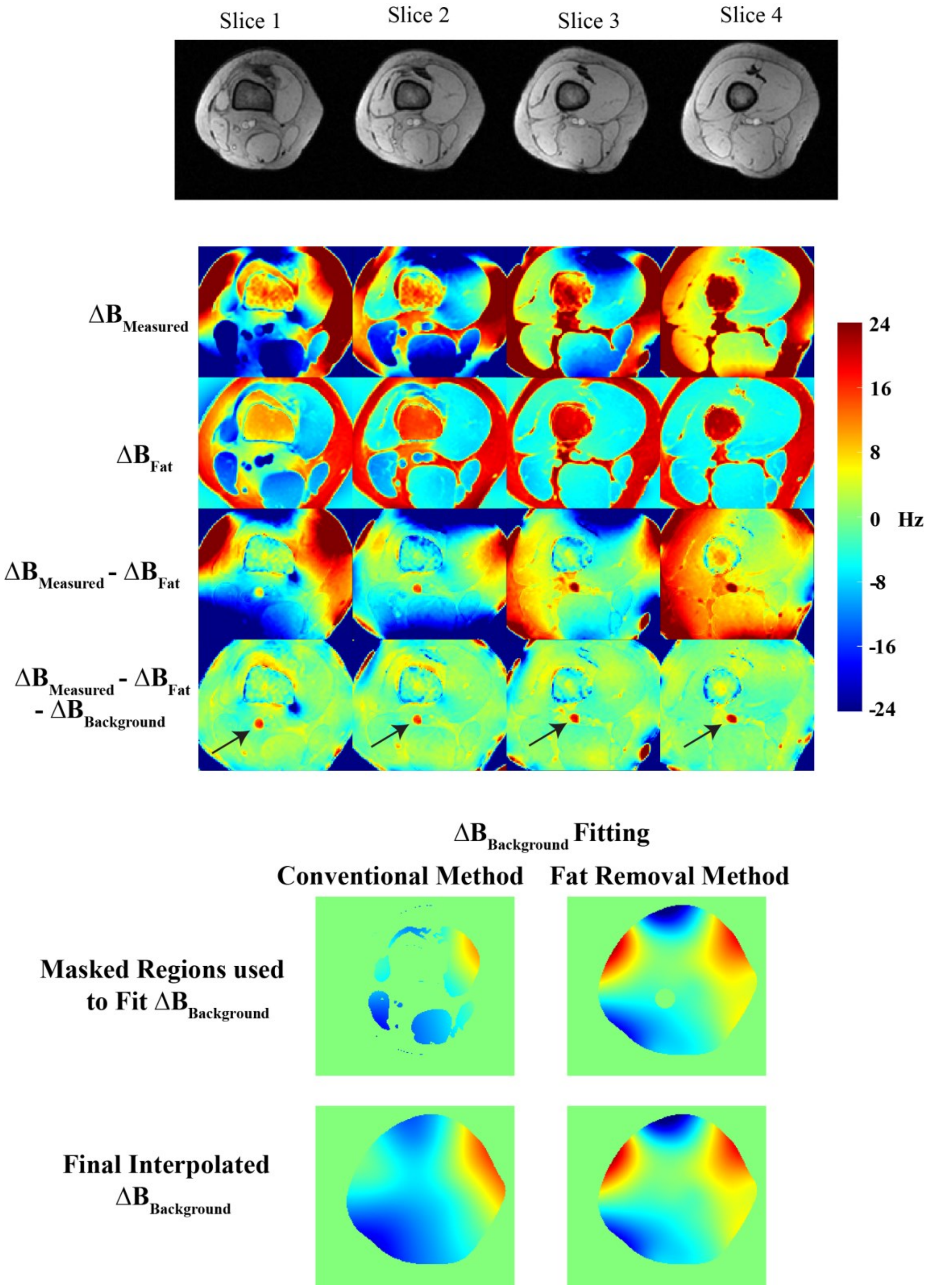

Figure 2.4 - (Top) Four sample slices from a multi-slice multi-echo Dixon acquisition (49 slices, 4mm slice thickness, no gap). The measured off-resonance field ($\Delta B_{Measured}$), the calculated off-

resonance field from the susceptibility of fat ($\Delta B_{Fat(\chi)}$), and the corrected fields, with removal of fat effects and the background field effects ($\Delta B_{Background}$), is shown for the four slices (**Middle**). Two methods for estimation of the background field are compared, highlighting the tissue regions used for fitting the background (**Bottom**). The conventional method uses only the muscle regions while the proposed fat-corrected method uses all tissue regions outside of the targeted vein region.

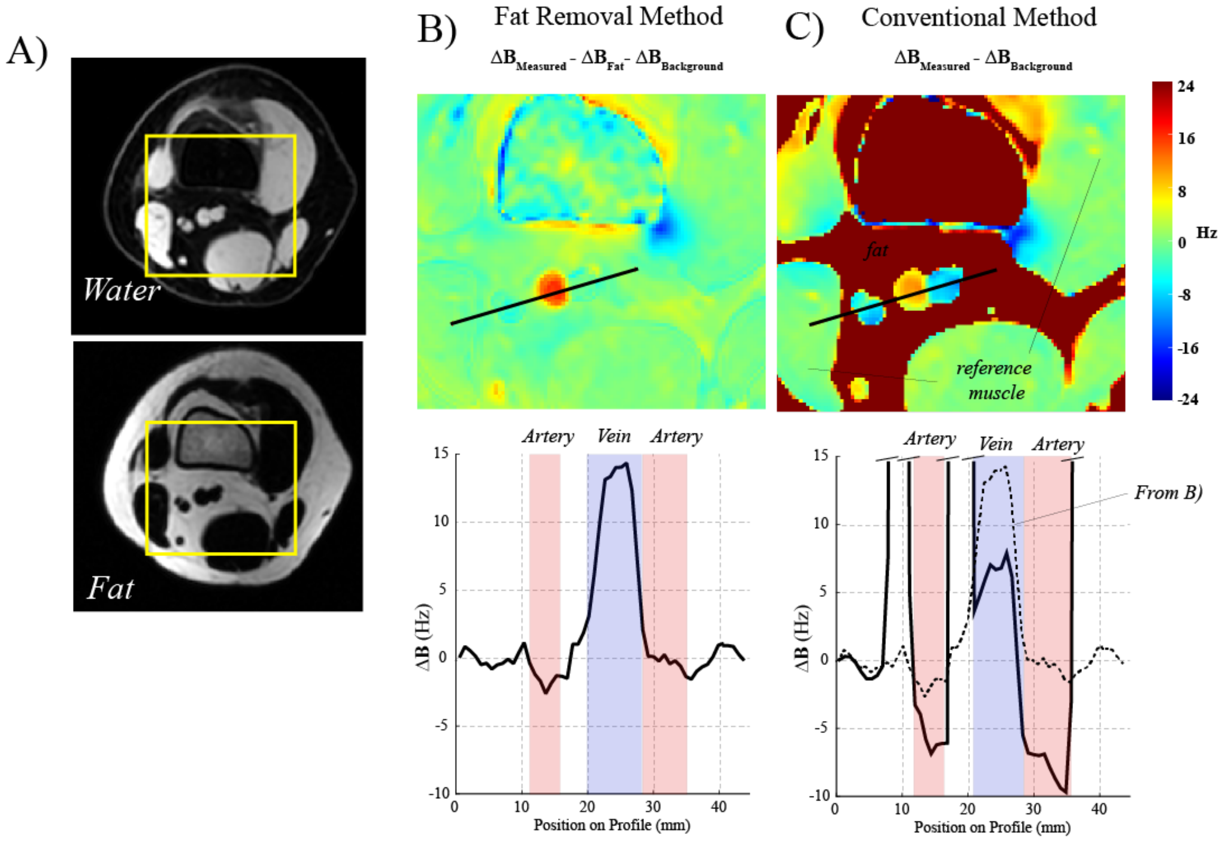

Figure 2.5 - (**A**) Fat and water separated images from a multi-slice multi-echo Dixon acquisition (same subject in Fig. 2.4). (**B**) A profile of the final calculated off-resonance field in the popliteal vein, ΔB_{O2}, using the proposed fat-correction method. (**C**) A profile of the final calculated off-resonance field in the popliteal vein, ΔB_{O2}, using the conventional method highlights the significant offset (reduced values in the vein and artery) as compared to the fat-corrected data.

2.3.2 Correction for Vein Angle Effects

The estimation of venous oxygen saturation (SvO_2) using the magnetic field shift within the vein, ΔB_{O2}, requires knowledge of the vein angle with respect to the main magnetic field; $SvO_2(\%)=100*[1-2*\Delta B_{O2}/(\gamma*\chi_{do*}Hct*B_{0*}(\cos^2\theta-1/3))]$. Figure 2.6 summarizes the measured vein angle over a 50 mm length of the popliteal vein in all 10 subjects, and the corresponding effect on calculated SvO_2 over this length, from the measured ΔB_{O2} values, illustrating more uniform oxygen saturation values after correction for angle effects. Average values for the 10 subjects are shown.

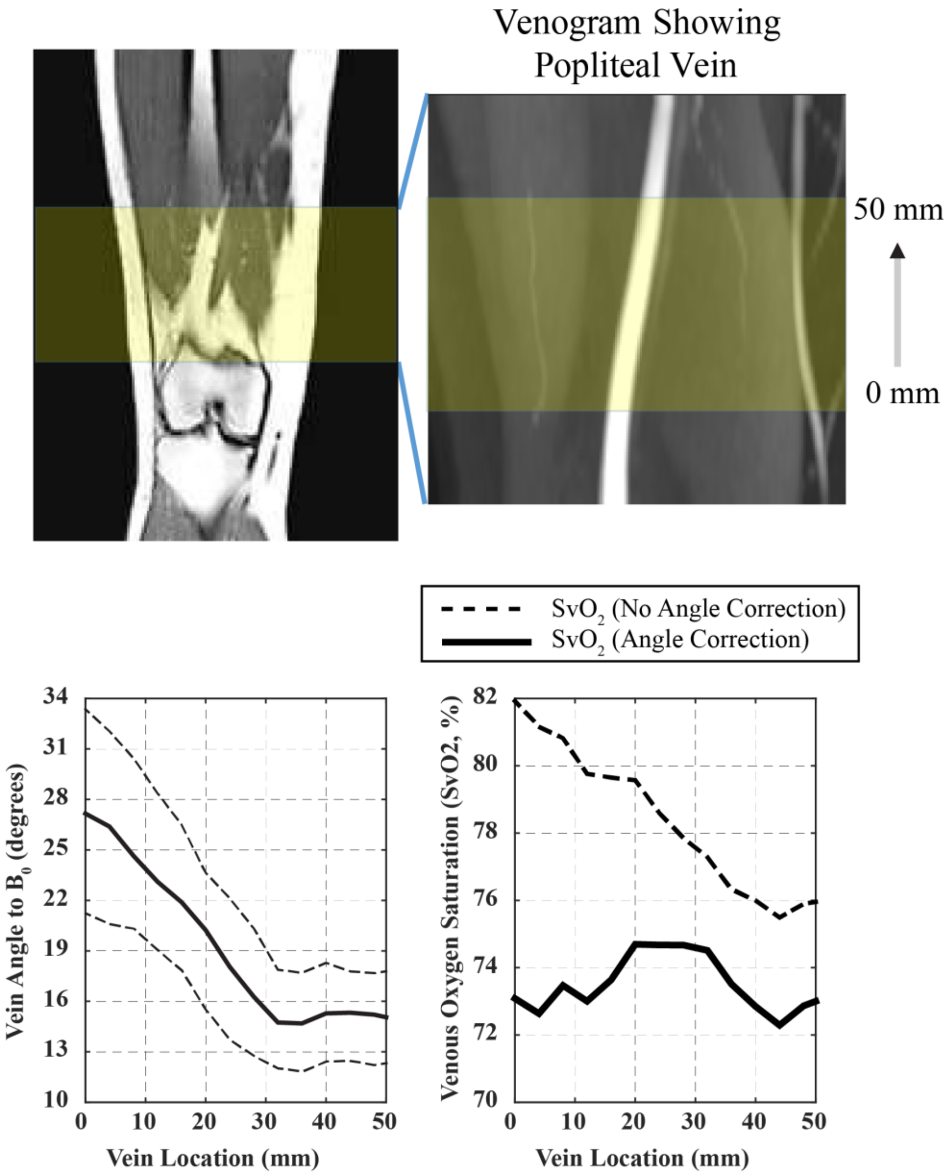

Figure 2.6 - (Top) A representative venogram shows the orientation of the popliteal vein in the targeted region superior to the knee in the lower thigh. The lower left plot shows the average vein angle to B_0 over a 50 mm length, beginning at the end of the gastrocnemius muscle group, just above the knee, and extending 50 mm superior (dashed lines show one standard deviation). The corresponding average SvO_2 values with and without correction for the vein angle are shown on the lower right.

2.3.3 Effects of Spatial Coverage on Calculation of ΔB_{Fat}

Figure 2.7 shows the change in the measured fat susceptibility field values in a targeted slice location as a function of spatial extent of the susceptibility values, $\chi_{Fat}(x,y,z)$, used to calculate ΔB_{Fat}. The sufficient spatial coverage will depend on the threshold for definition of negligible effects of additional slices. For this subject, a total z-oriented coverage of >12 cm will yield <1Hz change in the field location at any point. Similar results were observed for all subjects.

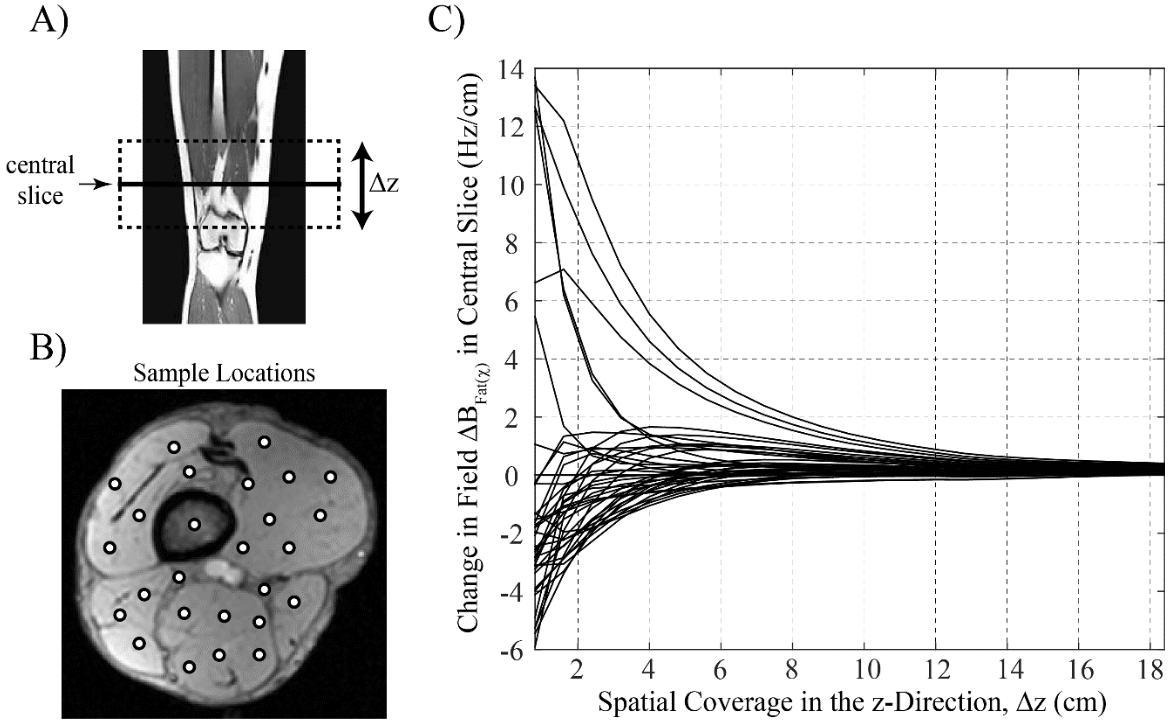

Figure 2.7 - The effects of spatial coverage of $\chi_{Fat}(x,y,z)$ in the z-direction, Δz, on the calculated ΔB_{Fat} in the central slice location, as shown in A) and B). The values plotted in C) show the change in the calculated field shift with inclusion of one addition slice on each end of the slab, in units of Hz/cm. Each plot in C) corresponds to a location in the central slice, as shown in B).

2.3.4 Exercise Studies

All 10 subjects completed plantar flexion exercise studies with assessment of resting (baseline) and post-exercise SvO_2 values, with results summarized in Table 2.1 and Figure 2.8 below. Results are shown for the dynamic single experiments, with correction for the fat-susceptibility effects measured from the corresponding multi-slice multi-echo acquisitions. The central slice from the multi-slice acquisitions match the location of the dynamic acquisitions. There was a significant difference in SvO_2 values between the conventional and fat-correction methods ($p<0.05$), with lower values for the conventional method (Table 2.1).

Table 2.1 Summary of SvO_2

Subject	**Gender**	**Vein angle (°)**	**SvO_2 (%) Fat-Correction Method**		**SvO_2 (%) Conventional Method**		**Difference between methods (%)**		**Maximum workload (Watts)**
			Baseline	Post-Exercise	Baseline	Post-Exercise	Baseline	Post-Exercise	
1	M	13.9	74.9	41.1	80.3	31.5	5.4	9.6	7.5
2	F	15.6	83.4	54.2	76.8	48.5	6.6	5.7	7.0
3	M	20.9	62.1	37.1	56.1	32.4	6	4.7	12.2
4	F	15.1	85.4	45.1	76.8	40.1	8.6	5.0	8.7
5	F	18.7	67.9	44.9	47.8	37.2	20.1	7.7	9.1
6	M	20.1	72.3	18.4	66.8	17.7	5.5	0.7	10.0
7	M	15.8	55	38.8	50.7	35.4	4.3	3.4	11.6
8	F	19.4	87.6	52.7	77.9	49.8	9.7	2.9	6.9
9	F	8.4	75.6	48.7	63.6	41.5	12	7.2	5.2
10	M	18.6	61.4	34.4	55.3	30.5	6.1	3.9	12.4
Average		16.7±3.7	72.6±11.0*	41.5±10.4*	65.2±12.2	36.5±9.4	7.4±6.4	5.1 ±2.6	9.1±2.5

*$p<0.05$ between fat-correction and conventional methods.

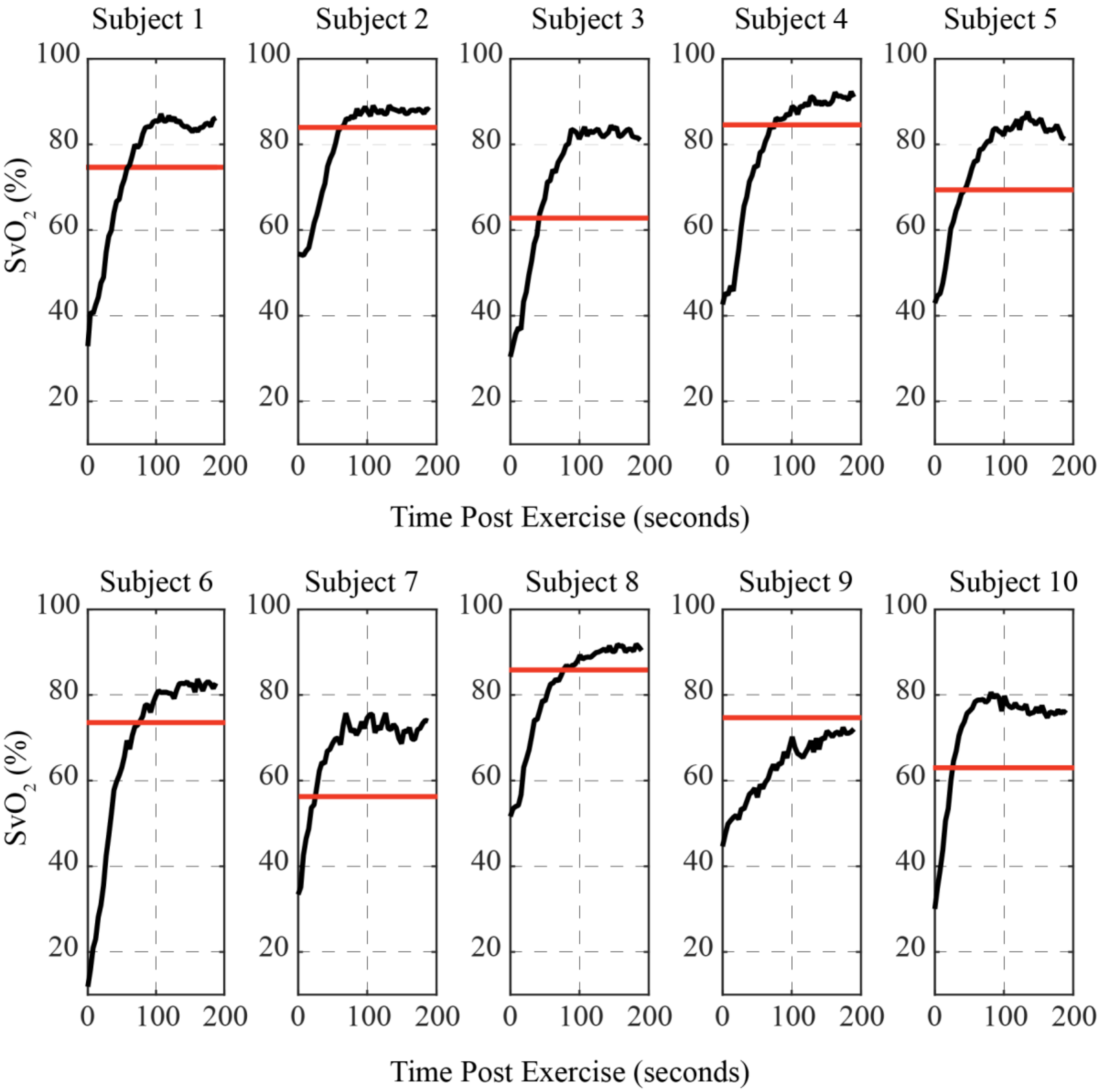

Figure 2.8 - SvO_2 baseline (rest values, red) and post-exercise recovery values (black) for all 10 study subjects. Peak and baseline values and workload data is summarized in Table 2.1 above.

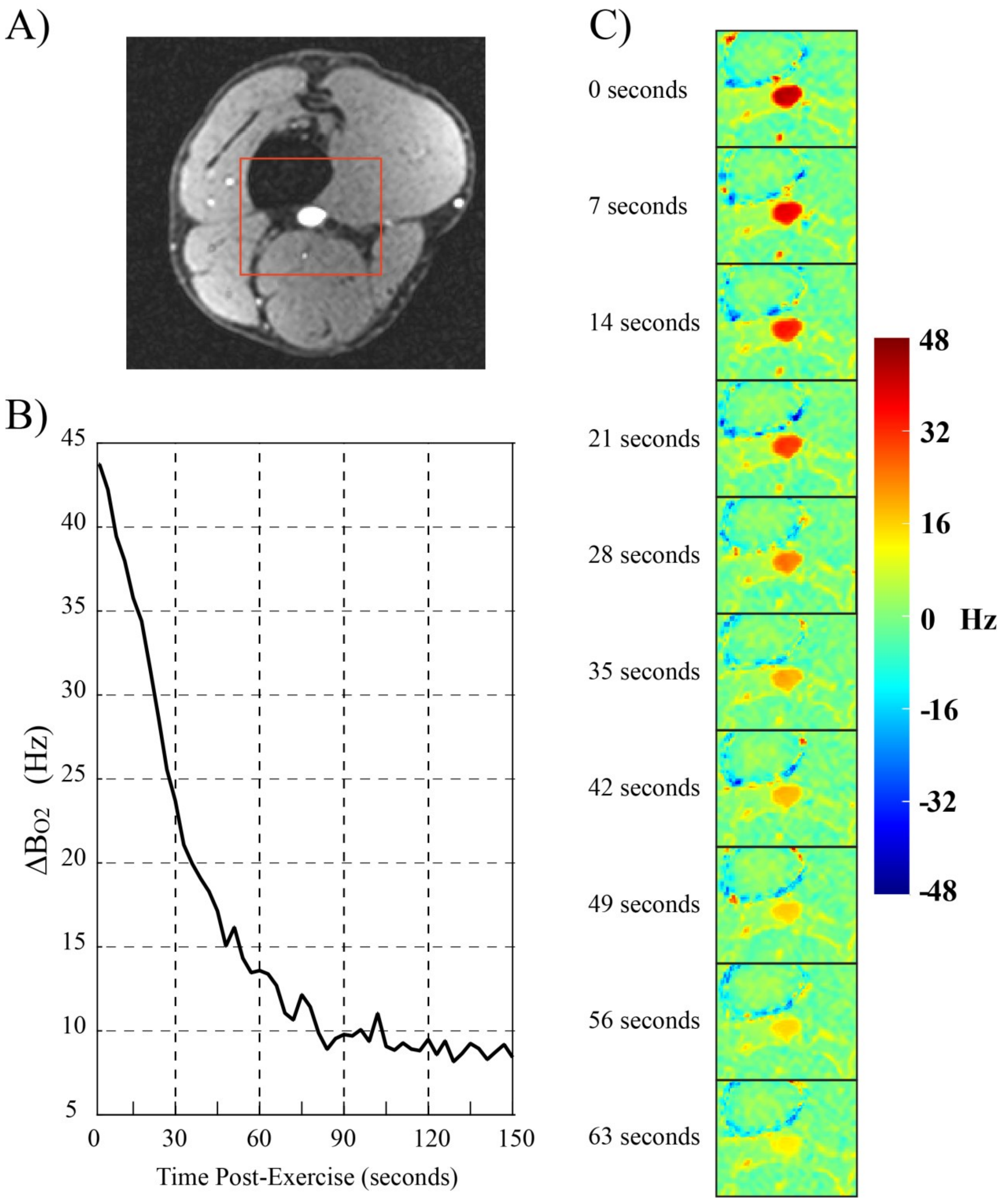

Figure 2.9 - (**A**) A water image from a fat-water separated Dixon acquisition. Post exercise time-resolved off-resonance frequency, ΔB_{O2}, in the popliteal vein with 10 sample time frames are shown in (**C**), from 50 measured times (**B**).

2.4 Discussion and Conclusions

The current study illustrated the effects of the magnetic susceptibility of fat on the static magnetic field within and surround the fat pool, showing relatively large fat-induced frequency offsets that can extend outside of the fat pool with relatively complex spatial patterns. These frequency offsets, $\Delta B_{Fat(\chi)}$, were shown to confound venous oxygen saturation (SvO_2) imaging methods that use the known offset in the venous susceptibility, and thus magnetic field shifts, as a function of deoxyhemoglobin concentration. Specifically, targeted measurement of the susceptibly-induced field shift within the vein, ΔB_{O2}, was confounded both by the local field inhomogeneities created by the fat as well as by the limited access to reference tissue near the vein, as a function of the thickness of the fat. Together, these factors made the necessary measurement and correction of the background magnetic field, $\Delta B_{Background}$, challenging and prone to error. Critically, the magnetic field shift in the vein must be calculated relative to the value of the background field at the location of the vein, which requires access to reference tissue as near as possible to the vein. Individuals with larger fat distributions, predominantly female subjects, had larger errors in calculated SvO_2, with an average shift of 11.4% in female subjects and 5.5% in male subjects ($p<0.05$ for gender comparison). It is well established that women generally have a higher proportion of body fat than men in both health and disease (85). The subject shown in Figure 2.9, with a small fat distribution, had a correspondingly small correction using the fat-correction method of 0.61 Hz. However, in general, the patient populations of interest, with unknown mechanisms of impaired exercise capacity, will be older and with risk factors such as obesity, so it is likely that large fat distributions will be the norm.

To address these challenges, a Dixon fat-water separation imaging approach was used to measure the distribution of fat, which enabled calculation and removal of the unwanted magnetic susceptibly effects of fat ($\Delta B_{Fat(\chi)}$), using the known susceptibility of fat. Additionally, the Dixon images provided the measured static magnetic field distribution with an intrinsic removal of the chemical shift effects of the fat ($\Delta B_{Fat(CS)}$), which enabled background magnetic field evaluation in fat as well as muscle regions surrounding the targeted vein. As was exemplified in Figures 2.4 and 2.5, the use of the predicted frequency shifts from fat, including both chemical shift and magnetic susceptibly effects, enabled their successful removal.

The differences between resting and post-exercise SvO_2 values for fat-correction (31.1±0.6%) and conventional method (28.7±2.8%) are similar which is expected because the same correction has been applied at rest and post-exercise, for each method. However, the absolute SvO_2 values are significantly higher ($p<0.05$) with the fat-correction method in a targeted central slice, both at rest and post exercise (Table 2.1). For the individual in Figure 2.5, the final calculated off-resonance field within the vein is approximately 14.5 Hz using the fat-correction method, while the conventional method yielded a lower off-resonance shift of 7 Hz. The corresponding SvO_2 values are 75.0% and 87.9%, for an absolute differences in SvO_2 of approximately 12.9%.

The average resting SvO_2 values in the 10 healthy volunteers were 72.6% using the proposed fat-correction method, which is similar to values reported in the popliteal vein (60%-80%) (86) and femoral vein (69.4%) (60). Similarly, the drop in SvO_2 immediately post-exercise in the current study to 41.5% is similar to that previous reported SvO_2 value in the femoral vein (42.1%) (60) and invasive catheter-derived SvO_2 value (42.3% at 10W) (17). During recovery from exercise, there is rapid recovery of SvO_2 values above resting values, as less oxygen is extracted (Figure 2.8). Post exercise SvO_2 overshoot, and thus further decreased oxygen extraction during recovery is likely the result of increased venous blood flow above resting values during this recovery period. Rapid recovery of SvO_2, and thus the field shift within the vein, following exercise, as shown in Figure 2.9, illustrates the requirement for good temporal resolution to resolve the peak values and rate of decay. Slowed recovery rates, in particular, are associated with impaired muscle function (68,87).

The SvO_2 imaging methods in the current study can be readily combined with venous blood flow imaging, as has previously been shown (27,60). Together, blood flow and oxygen extraction can be combined to derived muscle oxygen consumption, $VO_{2Muscle}$ (60,87). Importantly, the proposed methods are compatible with the dynamic exercise applications, which are essential for the study of the mechanisms of reduced exercise capacity (e.g. reduced oxygen extraction) in common conditions including diabetes, cancer, and heart failure.

In conclusion, it is necessary to correct for the magnetic susceptibility effects of fat in venous oxygen saturation imaging with increasing correction magnitude with increased fat thickness surrounding the targeted vein.

Chapter 3: Quantification of Skeletal Muscle Oxygen Consumption (VO_2) with Dynamic Exercise

3.1 Introduction

The volume of oxygen consumption (VO_2) is a quantitative measure of oxygen transport and extraction at the level of the tissues of the body. The maximum VO_2 during exercise (VO_{2max}) is the gold standard measure of exercise capacity, and is related directly to the cardiac output, the oxygen carrying capacity of the blood and the ability of muscle to extract the delivered oxygen. For example, patients with heart failure have significantly reduced VO_{2max}, which is the primary manifestation of their disease (e.g. inability to walk up a flight of stairs), due to the combined limitations of their heart, blood vessels and muscles (88,89). Whole body VO_{2max} is measured at the mouth, using the directly measured volume of oxygen consumed during exercise, typically in units of ml/kg/min (where kg refers to the whole body weight). However, this approach is limited in that it does not provide insight into the muscle-specific mechanisms of reduced exercise capacity. Furthermore, the peak values are most commonly used and not the rates of recovery back to resting values, which can provide additional information regarding muscle metabolism, where slowed rates of recovery are undesirable (68). Our goals are to measure isolated skeletal muscle oxygen consumption, $VO_{2muscle}$ with exercise, and the rates of recovery following exercise to enable the study of the muscle-specific limitations to reduced exercise capacity.

3.2 Methods

3.2.1 Measurement of Skeletal Muscle Oxygen Consumption

Skeletal muscle oxygen consumption was estimated from the Fick equation, as:

$$VO_{2Muscle} = VBF * Ca * Hgb * (SaO_2 - SvO_2) \qquad \text{Eq. 3.1}$$

where ca = 1.34 mL O_2/g of Hb (the oxygen carrying capacity of hemoglobin), and hemoglobin concentration in the blood was assumed to be 14.6 g/dL (with Hct = 0.43). Venous blood flow (VBF) was measured with a phase contrast MRI method targeting the popliteal vein (returning blood from the exercising calf muscles), at the same location used to estimate venous oxygen saturation (e.g. Figure 2.3). Arterial blood oxygen (SaO_2) was measured with a pulse oximeter placed on a finger and SvO_2 was estimated from MR susceptometry experiments as described in Chapter 2, for the estimation of oxygen extraction (SaO_2-SvO_2).

3.2.2 Pulse Sequence

All experiments were performed on a 3T MRI scanner (3T PRISMA; Siemens Healthcare; Erlangen, Germany). Acquisition parameters for the susceptometry acquisitions are given in section 2.2.6. Susceptometry acquisitions incorporate flow-compensation to ensure there is no motion-relation phase in the vein. To measure blood flow in the vein, each susceptomtery acquisition is repeated with identical parameters but with the addition of flow-encoding gradients, using a VENC of 50 cm/s. Each image is acquired in 1.93 seconds (102 k-space lines x 18.89 ms/line), for an effective temporal resolution of 1.93*2 = 3.86 seconds for both flow-encoding steps. The 18.89 ms TR includes an arterial saturation band, applied superior to the imaging plane to null the signal for the pulsatile arterial blood flow. The multi-gradient-echo pulse sequence is shown in Figure 3.1.

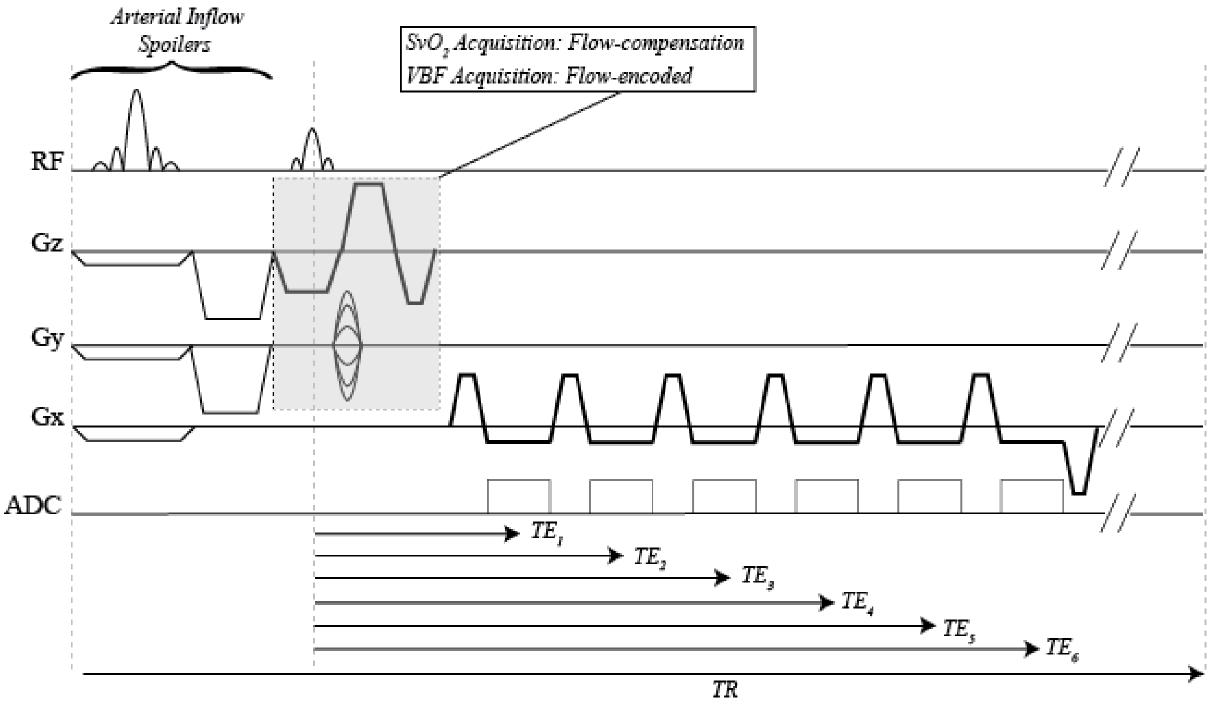

Figure 3.1 – The multi-gradient-echo pulse sequence used for evaluation of venous oxygen saturation and venous blood flow.

3.2.3 Exercise and Imaging Protocols

An MR-compatible exercise device (Trispect; Ergospect; Innsbruck, Austria) was used for plantar-flexion exercise, targeting the gastrocnemius muscle group in the calf. Plantar flexion exercise was performed against the resistance of the ergometer which is generated by programmable air pressure, to generate a targeted power (Watts). All subjects were placed in a supine position and their foot and ankle were fixed with the straps to the pedal of the ergometer (Figure 3.2). An audio exercise pacing signal sent to the subject's headphones was used to maintain the exercise rate during exercise (30 repetitions/minute). All subjects performed incremental exercise (4-9 Watts, increasing 1 Watt/minute) for 3-6 minutes, to a perceived level of 75% of maximum.

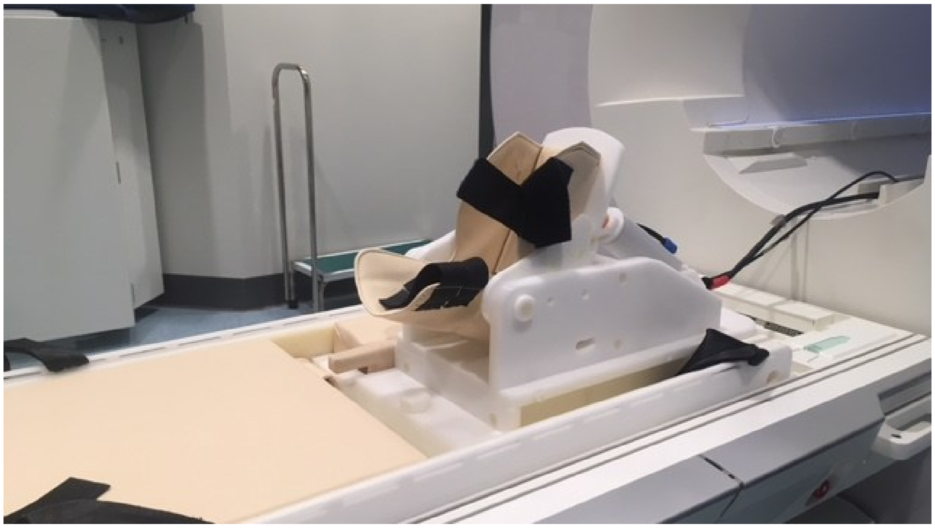

Figure 3.2 - MR compatible plantar-flexion exercise device.

Susceptometry acquisitions were interleaved with phase-contrast flow acquisitions with imaging duration of 1.93 s for each acquisition, or a repetition interval of 3.86 seconds. These images were repeated 20 times over 77.6 s for baseline (rest) and 50 times over 194 s after exercise. Exercise imaging started within one second of the completion of exercise to capture end-exercise peak values and recovery kinetics. In order to estimate VO_2 recovery time constant, τVO_2, the VO_2 time course data was fit with a mono-exponential decay function (90).

3.2.4 Subjects

Ten healthy subjects (5 male and 5 female; 27 ± 3 yrs; Body Mass Index, BMI, 21.2 ± 1.9 kg/m^2) provided written informed consent following an institutional review board-approved protocol. All subjects completed the exercise protocol.

3.2.5 Image Analysis

Figure 3.3 below shows a cross-section of popliteal vein in the first image immediately post exercise in a representative subject (gray colormap on top and jet colormap on bottom). From the time-resolved phase-contrast (left) and ΔB_{O2} (right) which were repeated 20 times at baseline and 50 times post exercise, the flow and susceptibility-induced magnetic field shifts were measured in a region of interest (ROI) placed at the center of the vessel. ΔB_{O2} values were converted to SvO_2 values using Eq. 2.1, incorporating the vein angle and hematocrit values. Hematocrit was assumed to be 0.43 for all subjects (91). The ROI was carefully placed to include all flow pixels, to capture the total flow through the vein, while the edge pixels were avoided on ΔB_{O2} images to mitigate partial volume errors (a single uniform value is expected).

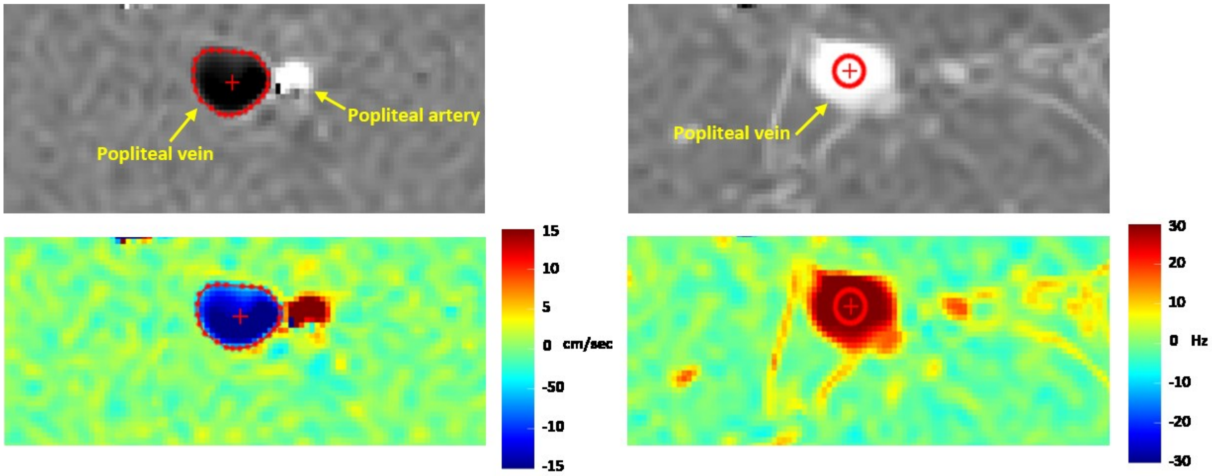

Figure 3.3 - Sample phase-contrast (left) and ΔB_{O2} images (right) immediately post exercise. Grayscale images (top) and color images (bottom).

3.2.6 Muscle Mass Quantification

The boundaries of gastrocnemius muscle were manually traced in each water images as defined in an IMAIOS e-Anatomy Atlas. The volume contained within this 3D region was multiplied by muscle density (1.06 g/mL) to provide an estimate of the muscle mass (kg). This muscle mass was used to normalize venous blood flow and skeletal muscle VO_2 to the mass of exercising gastrocnemius muscle group, which is the predominant muscle group activate for plantar flexion exercise. Acquisitions for muscle mass calculations used a multi-slice multi echo acquisition with 36 slices and 8 mm slice thickness, 192 x 102 acquisition matrix, 280 x 149 mm field of view, 1445 Hz/pixel receiver bandwidth, TR/TE = 702 ms/1.89 ms for a total scan time of 71.6s.

3.3 Results

Figure 3.4 shows a sample image, from 36 slices covering the entire calf muscle, with the manually traced gastrocnemius muscle. The average gastrocnemius muscle mass was 288 ± 90g. Figure 3.5 shows SvO_2, popliteal vein blood flow and calculated VO_2 time-curves following exercise in all subjects, with a summary of the average rest and peak values in Table 3.1. All data are reported as mean ± standard deviation. Table 3.2 summarizes all other measured parameters in all subjects. On average, peak exercise blood flow increased about 6 times over the baseline and venous oxygen saturation decreased from 73% to 42% with exercise. The mean baseline and peak exercise oxygen consumption were 12.5 mL/min/kg and 207.4 mL/min/kg, respectively. The average oxygen consumption recovery time constant following exercise was 29.9 seconds.

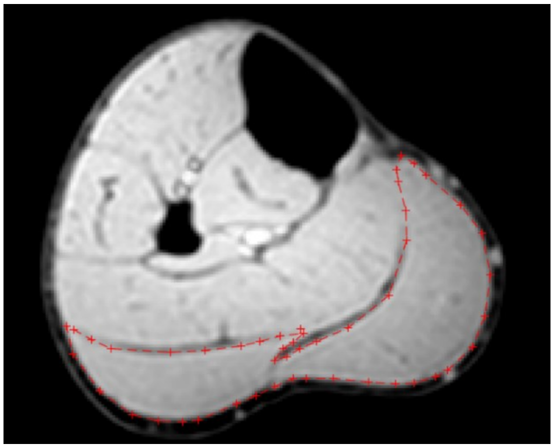

Figure 3.4 - A sample image (from 36 slices) used define the gastrocnemius muscle group for quantification of muscle mass.

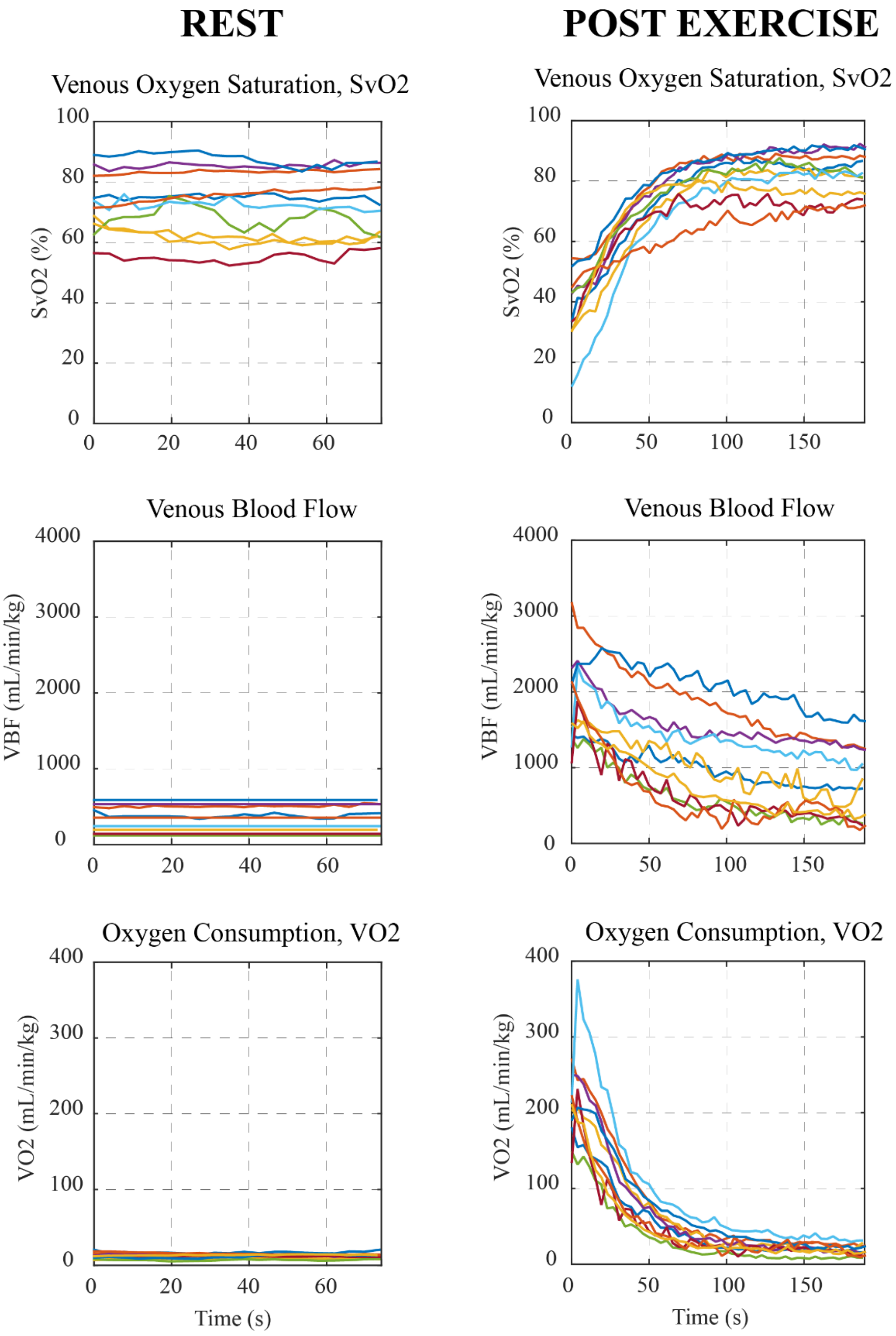

Figure 3.5- Dynamic data from all volunteers showing venous oxygen saturation (SvO_2), venous blood flow (VBF), and oxygen consumption (VO_2) following plantar flexion exercise. VBF and VO_2 are normalized to the gastrocnemius muscle mass.

Table 3.1 Summary of average data from exercise studies (mean ± std)

Subjects (N=10)	**Baseline**	**Post Exercise (Peak)**
Muscle Mass (kg)	0.2879 ± 0.09	
VBF (mL/min/kg)	317.1 ± 179.4	1917.8 ± 489.5
SvO_2 (%)	72.6 ± 11.0	41.5 ± 10.4
VO_2 (mL/min/kg)	12.5 ± 3.0	207.4 ± 50.7
τVO_2 (s)	29.9 ± 7.1	

Muscle mass is for gastrocnemius muscle group. VBF: venous blood flow; SvO_2: venous oxygen saturation; VO_2: oxygen consumption; τVO_2: oxygen consumption recovery time constant following exercise.

Table 3.2 - Summary of exercise data for each subject

Subject	Gender	Muscle Mass (Kg)	Vein angle (°)	VBF (mL/min/kg)		SvO_2 (%)		VO_2 (mL/min/kg)		τVO_2 (s)	Maximum workload (W)
				Rest	Post Ex	Rest	Post Ex	Rest	Post Ex		
1	M	0.24	13.9	379.0	1401.9	74.9	41.1	17.1	156.0	42.2	7.5
2	F	0.16	15.6	504.9	2843.4	83.4	54.2	14.4	243.8	33.6	7.0
3	M	0.46	20.9	192.7	1567.4	62.1	37.1	13.6	186.5	20.7	12.2
4	F	0.27	15.1	532.5	2348.0	85.4	45.1	13.1	243.0	26.5	8.7
5	F	0.26	18.7	117.9	1318.9	67.9	44.9	6.9	136.9	25.5	9.1
6	M	0.33	20.1	243.1	2113.0	72.3	18.4	12.2	314.4	27.2	10.0
7	M	0.31	15.8	140.4	1783.3	55.0	38.8	11.8	207.1	20.9	11.6
8	F	0.21	19.4	586.4	2371.2	87.6	52.7	11.9	210.1	31.3	6.9
9	F	0.21	8.4	353.7	1823.6	75.6	48.7	15.5	176.2	31.1	5.2
10	M	0.41	18.6	120.8	1607.5	61.4	34.4	8.7	200.1	39.3	12.4
Ave.		0.2879 ± 0.09	16.7 ± 3.7	317.1 ± 179.4	1917.8 ± 489.5	72.6 ± 11.0	41.5 ± 10.4	12.5 ± 3.0	207.4 ± 50.7	29.9 ± 7.1	9.1 ± 2.5

Muscle mass is for gastrocnemius muscle group. VBF: venous blood flow; SvO_2: venous oxygen saturation; VO_2: muscle oxygen consumption. τVO_2: oxygen consumption recovery time constant following exercise.

The venous oxygen content at rest and post exercise are plotted versus the gastrocnemius muscle mass in Figure 3.6. A significant ($p<0.05$) linear relationship between venous oxygen saturation and muscle was observed both at rest and post-exercise.

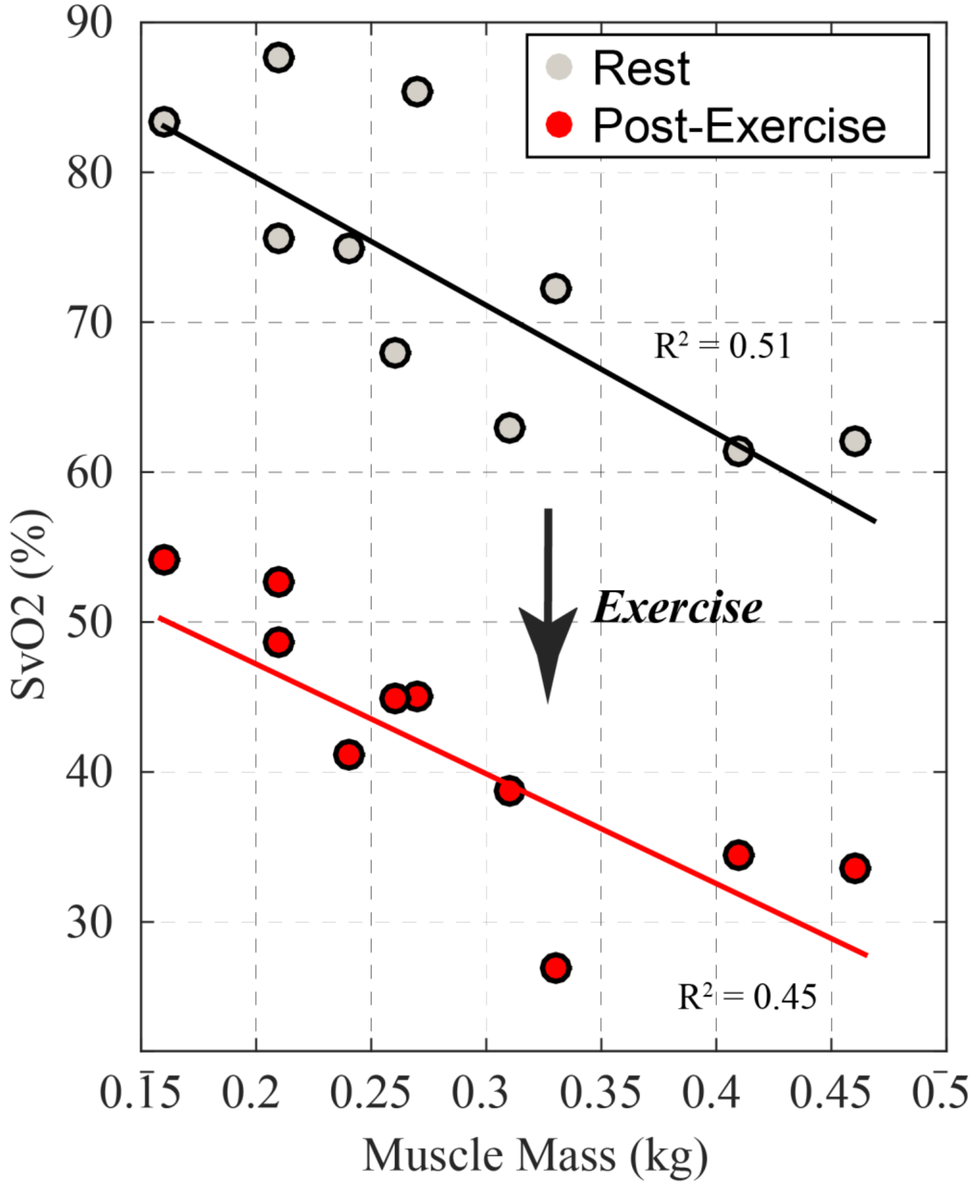

Figure 3.6 - Relationship between venous oxygen saturation (SvO_2, %) in the popliteal vein and gastrocnemius muscle mass in 10 healthy controls. A significant linear relationship ($p<0.05$) is observed for resting and post-exercise data.

3.4 Discussion and Conclusions

We have shown that simultaneous measurement of venous blood flow and oxygen saturation (SvO_2) with MRI is feasible in combination with isolated muscle (plantar flexion) exercise. Together, these two parameters enable estimation of oxygen consumption (VO_2) based on the Fick equation. Measurement of oxygen consumption in an isolated muscle, as opposed to the widely available whole body VO_2 test, is important to provide information about the muscle-specific mechanisms of reduced exercise capacity, removing the heart and great vessels (e.g. aorta) as potential contributing factors to reduced whole body VO_2. The presented methods are compatible with imaging during rapid recovery blood flow, SvO_2 and VO_2, with a temporal resolution of <4 seconds, which is sufficient to characterize the dynamics of all of these parameters over the recovery phase of the exercise challenge (67,92). The end-exercise values, at the onset of recovery, are acquired within 1 second of exercise completion, which are used a surrogate for peak exercise values.

At rest, the normal range of SvO_2 is fairly large, spanning 50-75% (17,27,62), with even larger resting SvO_2 values in the current study. Figure 3.6, which compares muscle mass and SvO_2, shows that the range of SvO_2 values observed in health is significantly related to the muscle mass, both at rest and with exercise. These results suggest that muscle mass is a major contributor to oxygen extraction, where increased absolute mass is associated with more extraction (lower SvO_2 values). It is possible that the larger capillary surface area in a larger muscle mass could be responsible for the larger oxygen extraction, and thus lower SvO_2, although we have no direct evidence to support this. After exercise, muscle oxygen consumption decreases rapidly back to normal levels, with time constant of ~30 seconds (Table 3.2), but blood flow remains above resting levels for several minutes (Figure 3.5). Oxygen extraction decreases rapidly to values below the resting levels (i.e. higher SvO_2 values than at rest). This shows that the blood flow is not directly regulated by the oxygen delivery to the contracting skeletal muscle (93). It is likely that increased blood flow reflects reduced vascular resistance, which is maintained following exercise, and the reduction in muscle oxygen extraction during recovery is the consequence of near resting VO_2 values. In other words, because the requirement for oxygen consumption recovers more rapidly than blood flow, the result is reduced oxygen extraction (higher SvO_2 values).

The VO_2 recovery time constant after exercise is not strongly related to workload intensity (90). It also provides important clinical information as the prolonged τVO_2 is directly related to disease severity in heart failure patients (65,94,95). The τVO_2 is significantly delayed in heart failure patients, with values as long as 95 seconds (87). The muscle τVO_2 in the current study of ~30 seconds in young heathy subjects is similar to the previous reported value, 26 seconds (60) and 33 seconds (90) during dynamic isolated muscle exercise. This metric has the advantage over the peak value at a single time point of being less sensitive to the peak work load achieved. For example, in Table 3.2, subject 4 and 5 have similar muscle mass (0.27 and 0.26 kg) and performed almost the same exercise workloads (8.7 and 9.1W). However, their exercise workloads are potentially not the same fraction of their peak workload intensity, which was not determined. Thus, their differences in peak blood flow and oxygen consumption values could be related to differences in relative workload.

In conclusion, we demonstrate that it is feasible to measure blood flow and oxygen saturation simultaneously at rest and immediately post-exercise in the popliteal vein to assess total skeletal muscle oxygen consumption. The establishment of this set of tools will enable to the study of the skeletal muscle mechanisms of reduced exercise capacity in numerous conditions, including heart failure, liver disease, diabetes, and obesity and with cancer therapies (chemotherapy and radiation), among many others.

Chapter 4: Conclusions and Future Directions

4.1 Summary of the Findings

The primary goal of this thesis was to measure and correct for the unwanted magnetic susceptibility effects of fat in venous oxygen saturation imaging and to illustrate the application for lower leg muscle oxygen consumption (VO_2) with plantar flexion exercise with MRI.

We showed that the susceptibility effects of fat extend outside of the fat pool and have the potential to confound the assessment of venous oxygen saturation based on magnetic susceptibility of deoxyhemoglobin.

We have developed and evaluated a new MRI method for the quantification and correction of the magnetic susceptibility effects of fat on the blood vessels contained within fat. A rapid fat-water separation imaging method is used to generate patient-specific magnetic susceptibility models to allow for separation of the underlying venous susceptibility that is used to quantify oxygen saturation in the vein from the unwanted contamination fields including main field inhomogeneity and susceptibility effects from fat. Measurement and removal of both the chemical shift and magnetic susceptibility field shift effects of fat allow the fat pool to be included with the muscle as a reference tissue, for measurement and removal of the static field inhomogeneity (background field), which is necessary to define the field arising from deoxyhemoglobin alone.

These imaging methods also allow for simultaneous quantification of venous blood flow which is used in conjunction with venous oxygen saturation to estimate total oxygen consumption. We have applied this new method to directly measure blood oxygenation and blood flow *in vivo* in the popliteal vein with plantar flexion exercise to estimate the whole lower leg muscle oxygen consumption. The effective temporal resolution of 3.86 s was sufficient to measure the dynamics of all parameters. Resting and post-exercise SvO_2 values in the 10 healthy subjects were 72.6% and 41.5%, respectively, which are similar to values previous reported in the femoral vein, 42.1% (60,86).

4.2 Study Limitations and Future Directions

The susceptometry methods used here rely on the shape of the vessel and its orientation relative to the external magnetic field. If the long cylinder is oriented parallel to the external field, the magnetic field in the surrounding material will be equal to its external magnetic field. Noncircular cross-section, curvature and complex branching of the vein produce deviations from cylindrical geometry, causing errors in venous oxygen saturation estimation (53,96). The popliteal vein has circular cross-section (Figure 2.4), but it shows curvature along its path (Figure 2.6) and tapering with several bifurcations (both in superior and inferior). Therefore, the location of the imaging slice along the popliteal vein (the location at which venous oxygen saturation is estimated) is important.

The whole lower leg muscle oxygen consumption is estimated based on the flow and oxygen content in the popliteal vein which returns blood from calf muscle. However, not all muscle groups perform exercise with plantar flexion exercise, which more specifically targets the gastrocnemius muscle groups. Thus, the oxygen content and blood flow in sampled venous blood pool is a weighted average from all muscle groups below the knee. However, the muscle groups that perform more intense exercise will dominate the flow and thus the oxygen content of the popliteal vein. In addition, imaging during exercise is currently not possible due to motion artifacts and thus, the on-transient kinetics of oxygen uptake cannot be measured.

Not all 10 subjects included in the current studies performed the same absolute exercise work intensity. All subjects performed incremental plantar flexion exercise with a goal of 75% of maximal effort. More accurate methods are needed to determine each subject's peak work load. In future studies, phosphocretine (PCr) and pH changes during and after exercise can be used as indicators.

We also assume a hematocrit of 0.43 for all subjects. However, the average hematocrit for women is 0.39 (0.36-0.48) and 0.44 (0.40-0.54) for men (97). Blood samples should be used in future study to calculate venous oxygen saturation accurately.

Bone can cause additional errors by producing an inhomogeneous field due to a different susceptibility than water by -2.39 ppm (98). Background field variations are usually low spatial frequency. Several methods including shimming and polynomial fitting can be used to remove these background variations (86,99). The inverse problem can also be used to remove the background field and to quantify the magnetic susceptibility from MR phase images (37,70,72,100,101). However, the inverse problem is more complicated and has limitations when applying to exercise studying. The measurements of blood flow and venous oxygen saturation in resting and post-exercise were performed using the interleaved 2D gradient echo sequence. However, the input image for reconstructing the susceptibility map needs to be 3D gradient echo sequence, demanding longer imaging times that are not compatible with dynamic time-resolved experiments (72).

The relationship between the oxygen consumption recovery kinetics and ATP re-synthesis (ADP + Inorganic phosphate, P_i) is unknown. In future studies, phosphorus-31 nuclear magnetic resonance spectroscopy can be combined with our proposed methods to study skeletal muscle metabolism at the cellular level.

4.3 Conclusions

The magnetic susceptibility of fat gives rise to potentially complex variations in the static magnetic field in skeletal muscle, which was shown to give rise to errors in the estimated venous oxygen saturation. On a subject-by-subject basis, Dixon fat-water separated imaging can be used to measure the distribution of fat and to correct the susceptibility effects of fat, while also measuring the targeted magnetic field which is used to estimate venous oxygen saturation. These methods are compatible with the targeted dynamic exercise applications, which are essential for the study of the mechanisms of reduced exercise capacity, independent of heart function, including reduced oxygen extraction, blood flow or delayed recovery following exercise (68).

References

1. Gulati M, Pandey DK, Arnsdorf MF, Lauderdale DS, Thisted RA, Wicklund RH, Al-Hani AJ, Black HR. Exercise capacity and the risk of death in women: the St James Women Take Heart Project. Circulation 2003;108(13):1554-1559.

2. Myers J, Prakash M, Froelicher V, Do D, Partington S, Atwood JE. Exercise capacity and mortality among men referred for exercise testing. The New England journal of medicine 2002;346(11):793-801.

3. Gallagher D, Belmonte D, Deurenberg P, Wang Z, Krasnow N, Pi-Sunyer FX, Heymsfield SB. Organ-tissue mass measurement allows modeling of REE and metabolically active tissue mass. The American journal of physiology 1998;275(2 Pt 1):E249-258.

4. Meyer RA, Towse TF, Reid RW, Jayaraman RC, Wiseman RW, McCully KK. BOLD MRI mapping of transient hyperemia in skeletal muscle after single contractions. NMR in biomedicine 2004;17(6):392-398.

5. Jacobi B, Bongartz G, Partovi S, Schulte AC, Aschwanden M, Lumsden AB, Davies MG, Loebe M, Noon GP, Karimi S, Lyo JK, Staub D, Huegli RW, Bilecen D. Skeletal muscle BOLD MRI: from underlying physiological concepts to its usefulness in clinical conditions. Journal of magnetic resonance imaging : JMRI 2012;35(6):1253-1265.

6. Richardson RS, Grassi B, Gavin TP, Haseler LJ, Tagore K, Roca J, Wagner PD. Evidence of O2 supply-dependent VO2 max in the exercise-trained human quadriceps. Journal of applied physiology 1999;86(3):1048-1053.

7. Richardson RS, Wary C, Wray DW, Hoff J, Rossiter HB, Layec G, Carlier PG. MRS Evidence of Adequate O(2) Supply in Human Skeletal Muscle at the Onset of Exercise. Medicine and science in sports and exercise 2015;47(11):2299-2307.

8. Welch HG, Bonde-Petersen F, Graham T, Klausen K, Secher N. Effects of hyperoxia on leg blood flow and metabolism during exercise. Journal of applied physiology: respiratory, environmental and exercise physiology 1977;42(3):385-390.

9. West JB. Pulmonary physiology and pathophysiology : an integrated, case-based approach. Philadelphia: Wolters Kluwer Health/Lippincott Williams & Wilkins; 2007. vii, 150 p. p.

10. DeLorey DS, Paterson DH, Kowalchuk JM. Effects of ageing on muscle O2 utilization and muscle oxygenation during the transition to moderate-intensity exercise. Applied physiology, nutrition, and metabolism = Physiologie appliquee, nutrition et metabolisme 2007;32(6):1251-1262.

11. Tortora GJ, Derrickson B. Introduction to the human body : the essentials of anatomy and physiology. New York: John Wiley & Sons; 2010. xxiv, 624, 625, 629, 622, 619 p. p.

12. Romijn JA, Coyle EF, Sidossis LS, Gastaldelli A, Horowitz JF, Endert E, Wolfe RR. Regulation of endogenous fat and carbohydrate metabolism in relation to exercise intensity and duration. The American journal of physiology 1993;265(3 Pt 1):E380-391.

13. Withers RT, Sherman WM, Clark DG, Esselbach PC, Nolan SR, Mackay MH, Brinkman M. Muscle metabolism during 30, 60 and 90 s of maximal cycling on an air-braked ergometer. European journal of applied physiology and occupational physiology 1991;63(5):354-362.

14. Sahlin K. Muscle fatigue and lactic acid accumulation. Acta physiologica Scandinavica Supplementum 1986;556:83-91.

15. Kety SS, Schmidt CF. The Nitrous Oxide Method for the Quantitative Determination of Cerebral Blood Flow in Man: Theory, Procedure and Normal Values. The Journal of clinical investigation 1948;27(4):476-483.

16. Mayberg TS, Lam AM. Jugular bulb oximetry for the monitoring of cerebral blood flow and metabolism. Neurosurgery clinics of North America 1996;7(4):755-765.

17. Andersen P, Saltin B. Maximal perfusion of skeletal muscle in man. The Journal of physiology 1985;366:233-249.

18. Mintun MA, Raichle ME, Martin WR, Herscovitch P. Brain oxygen utilization measured with O-15 radiotracers and positron emission tomography. Journal of nuclear medicine : official publication, Society of Nuclear Medicine 1984;25(2):177-187.

19. Ito H, Ibaraki M, Kanno I, Fukuda H, Miura S. Changes in cerebral blood flow and cerebral oxygen metabolism during neural activation measured by positron emission tomography: comparison with blood oxygenation level-dependent contrast measured by functional magnetic resonance imaging. Journal of cerebral blood flow and metabolism : official journal of the International Society of Cerebral Blood Flow and Metabolism 2005;25(3):371-377.

20. Baron JC, Jones T. Oxygen metabolism, oxygen extraction and positron emission tomography: Historical perspective and impact on basic and clinical neuroscience. NeuroImage 2012;61(2):492-504.

21. Kudomi N, Hirano Y, Koshino K, Hayashi T, Watabe H, Fukushima K, Moriwaki H, Teramoto N, Iihara K, Iida H. Rapid quantitative CBF and CMRO(2) measurements from a single PET scan with sequential administration of dual (15)O-labeled tracers. Journal of cerebral blood flow and metabolism : official journal of the International Society of Cerebral Blood Flow and Metabolism 2013;33(3):440-448.

22. Frackowiak RS, Lenzi GL, Jones T, Heather JD. Quantitative measurement of regional cerebral blood flow and oxygen metabolism in man using 15O and positron emission tomography: theory, procedure, and normal values. Journal of computer assisted tomography 1980;4(6):727-736.

23. Daubeney PE, Pilkington SN, Janke E, Charlton GA, Smith DC, Webber SA. Cerebral oxygenation measured by near-infrared spectroscopy: comparison with jugular bulb oximetry. The Annals of thoracic surgery 1996;61(3):930-934.

24. Mozina H, Podbegar M. Near-infrared spectroscopy for evaluation of global and skeletal muscle tissue oxygenation. World journal of cardiology 2011;3(12):377-382.

25. Jobsis FF. Noninvasive, infrared monitoring of cerebral and myocardial oxygen sufficiency and circulatory parameters. Science 1977;198(4323):1264-1267.

26. Van Beekvelt MC, Colier WN, Wevers RA, Van Engelen BG. Performance of near-infrared spectroscopy in measuring local O(2) consumption and blood flow in skeletal muscle. Journal of applied physiology 2001;90(2):511-519.

27. Langham MC, Floyd TF, Mohler ER, 3rd, Magland JF, Wehrli FW. Evaluation of cuff-induced ischemia in the lower extremity by magnetic resonance oximetry. Journal of the American College of Cardiology 2010;55(6):598-606.

28. Tortoriello TA, Stayer SA, Mott AR, McKenzie ED, Fraser CD, Andropoulos DB, Chang AC. A noninvasive estimation of mixed venous oxygen saturation using near-infrared spectroscopy by cerebral oximetry in pediatric cardiac surgery patients. Paediatric anaesthesia 2005;15(6):495-503.

29. Lu H, Ge Y. Quantitative evaluation of oxygenation in venous vessels using T2-Relaxation-Under-Spin-Tagging MRI. Magnetic resonance in medicine 2008;60(2):357-363.

30. Xu F, Ge Y, Lu H. Noninvasive quantification of whole-brain cerebral metabolic rate of oxygen (CMRO2) by MRI. Magnetic resonance in medicine 2009;62(1):141-148.

31. Jain V, Magland J, Langham M, Wehrli FW. High temporal resolution in vivo blood oximetry via projection-based T2 measurement. Magnetic resonance in medicine 2013;70(3):785-790.

32. Wright GA, Hu BS, Macovski A. 1991 I.I. Rabi Award. Estimating oxygen saturation of blood in vivo with MR imaging at 1.5 T. Journal of magnetic resonance imaging : JMRI 1991;1(3):275-283.

33. Haacke EM, Lai S, Reichenbach JR, Kuppusamy K, Hoogenraad FG, Takeichi H, Lin W. In vivo measurement of blood oxygen saturation using magnetic resonance imaging: a

direct validation of the blood oxygen level-dependent concept in functional brain imaging. Human brain mapping 1997;5(5):341-346.

34. Fernandez-Seara MA, Techawiboonwong A, Detre JA, Wehrli FW. MR susceptometry for measuring global brain oxygen extraction. Magnetic resonance in medicine 2006;55(5):967-973.

35. Jain V, Langham MC, Wehrli FW. MRI estimation of global brain oxygen consumption rate. Journal of cerebral blood flow and metabolism : official journal of the International Society of Cerebral Blood Flow and Metabolism 2010;30(9):1598-1607.

36. Brown RW, Cheng Y-CN, Haacke EM, Thompson MR, Venkatesan R. Magnetic resonance imaging : physical principles and sequence design. 1 online resource. p.

37. Liu C, Li W, Tong KA, Yeom KW, Kuzminski S. Susceptibility-weighted imaging and quantitative susceptibility mapping in the brain. Journal of magnetic resonance imaging : JMRI 2015;42(1):23-41.

38. Thulborn KR, Waterton JC, Matthews PM, Radda GK. Oxygenation dependence of the transverse relaxation time of water protons in whole blood at high field. Biochimica et biophysica acta 1982;714(2):265-270.

39. Golay X, Silvennoinen MJ, Zhou J, Clingman CS, Kauppinen RA, Pekar JJ, van Zijl PC. Measurement of tissue oxygen extraction ratios from venous blood T(2): increased precision and validation of principle. Magnetic resonance in medicine 2001;46(2):282-291.

40. Stainsby JA, Wright GA. Partial volume effects on vascular T2 measurements. Magnetic resonance in medicine 1998;40(3):494-499.

41. Gati JS, Menon RS, Ugurbil K, Rutt BK. Experimental determination of the BOLD field strength dependence in vessels and tissue. Magnetic resonance in medicine 1997;38(2):296-302.

42. Jezzard P, Clare S. Sources of distortion in functional MRI data. Human brain mapping 1999;8(2-3):80-85.

43. Lu H, Xu F, Grgac K, Liu P, Qin Q, van Zijl P. Calibration and validation of TRUST MRI for the estimation of cerebral blood oxygenation. Magnetic resonance in medicine 2012;67(1):42-49.

44. Qin Q, Grgac K, van Zijl PC. Determination of whole-brain oxygen extraction fractions by fast measurement of blood T(2) in the jugular vein. Magnetic resonance in medicine 2011;65(2):471-479.

45. Zhao JM, Clingman CS, Narvainen MJ, Kauppinen RA, van Zijl PC. Oxygenation and hematocrit dependence of transverse relaxation rates of blood at 3T. Magnetic resonance in medicine 2007;58(3):592-597.

46. Detre JA, Alsop DC. Perfusion magnetic resonance imaging with continuous arterial spin labeling: methods and clinical applications in the central nervous system. European journal of radiology 1999;30(2):115-124.

47. Edelman RR, Siewert B, Darby DG, Thangaraj V, Nobre AC, Mesulam MM, Warach S. Qualitative mapping of cerebral blood flow and functional localization with echo-planar MR imaging and signal targeting with alternating radio frequency. Radiology 1994;192(2):513-520.

48. Xu F, Uh J, Liu P, Lu H. On improving the speed and reliability of T2-relaxation-under-spin-tagging (TRUST) MRI. Magnetic resonance in medicine 2012;68(1):198-204.

49. Christen T, Bolar DS, Zaharchuk G. Imaging brain oxygenation with MRI using blood oxygenation approaches: methods, validation, and clinical applications. AJNR American journal of neuroradiology 2013;34(6):1113-1123.

50. Rodgers ZB, Detre JA, Wehrli FW. MRI-based methods for quantification of the cerebral metabolic rate of oxygen. Journal of cerebral blood flow and metabolism : official journal of the International Society of Cerebral Blood Flow and Metabolism 2016;36(7):1165-1185.

51. Spees WM, Yablonskiy DA, Oswood MC, Ackerman JJ. Water proton MR properties of human blood at 1.5 Tesla: magnetic susceptibility, T(1), T(2), T*(2), and non-Lorentzian signal behavior. Magnetic resonance in medicine 2001;45(4):533-542.

52. Schenck JF. The role of magnetic susceptibility in magnetic resonance imaging: MRI magnetic compatibility of the first and second kinds. Medical physics 1996;23(6):815-850.

53. Langham MC, Magland JF, Epstein CL, Floyd TF, Wehrli FW. Accuracy and precision of MR blood oximetry based on the long paramagnetic cylinder approximation of large vessels. Magnetic resonance in medicine 2009;62(2):333-340.

54. Ho SS, Chan YL, Yeung DK, Metreweli C. Blood flow volume quantification of cerebral ischemia: comparison of three noninvasive imaging techniques of carotid and vertebral arteries. AJR American journal of roentgenology 2002;178(3):551-556.

55. Hundley WG, Li HF, Hillis LD, Meshack BM, Lange RA, Willard JE, Landau C, Peshock RM. Quantitation of cardiac output with velocity-encoded, phase-difference magnetic resonance imaging. The American journal of cardiology 1995;75(17):1250-1255.

56. Spilt A, Box FM, van der Geest RJ, Reiber JH, Kunz P, Kamper AM, Blauw GJ, van Buchem MA. Reproducibility of total cerebral blood flow measurements using phase contrast magnetic resonance imaging. Journal of magnetic resonance imaging : JMRI 2002;16(1):1-5.

57. Ramalho JN, Castillo M, Semelka RC. Vascular imaging of the central nervous system : physical principles, clinical applications and emerging techniques. 1 online resource (427 pages) p.

58. Ferr©*ndez JM. New challenges on bioinspired applications 4th International Work-conference on the Interplay Between Natural and Artificial Computation, IWINAC 2011, La Palma, Canary Islands, Spain, May 30 - June 3, 2011, Proceedings. Part II. Lecture notes in computer science 6687. Berlin ; Heidelberg ; New York: Springer; 2011. p xxvi, 486 p.

59. Gatehouse PD, Keegan J, Crowe LA, Masood S, Mohiaddin RH, Kreitner KF, Firmin DN. Applications of phase-contrast flow and velocity imaging in cardiovascular MRI. European radiology 2005;15(10):2172-2184.

60. Mathewson KW, Haykowsky MJ, Thompson RB. Feasibility and reproducibility of measurement of whole muscle blood flow, oxygen extraction, and VO2 with dynamic exercise using MRI. Magnetic resonance in medicine 2015;74(6):1640-1651.

61. Drake RL, Vogl W, Mitchell AWM, Tibbitts R, Richardson P, Horn A. Gray's basic anatomy. International ed. Philadelphia: Elsevier/Churchill Livingstone; 2012. p 1 online resource (xx, 610 p.).

62. Macmillan CS, Andrews PJ. Cerebrovenous oxygen saturation monitoring: practical considerations and clinical relevance. Intensive care medicine 2000;26(8):1028-1036.

63. Gademan MG, Swenne CA, Verwey HF, van de Vooren H, Haest JC, van Exel HJ, Lucas CM, Cleuren GV, Schalij MJ, van der Wall EE. Exercise training increases oxygen uptake efficiency slope in chronic heart failure. European journal of cardiovascular prevention and rehabilitation : official journal of the European Society of Cardiology, Working Groups on Epidemiology & Prevention and Cardiac Rehabilitation and Exercise Physiology 2008;15(2):140-144.

64. Hollenberg M, Tager IB. Oxygen uptake efficiency slope: an index of exercise performance and cardiopulmonary reserve requiring only submaximal exercise. Journal of the American College of Cardiology 2000;36(1):194-201.

65. Cohen-Solal A, Laperche T, Morvan D, Geneves M, Caviezel B, Gourgon R. Prolonged kinetics of recovery of oxygen consumption after maximal graded exercise in patients with chronic heart failure. Analysis with gas exchange measurements and NMR spectroscopy. Circulation 1995;91(12):2924-2932.

66. de Groote P, Millaire A, Decoulx E, Nugue O, Guimier P, Ducloux. Kinetics of oxygen consumption during and after exercise in patients with dilated cardiomyopathy. New markers of exercise intolerance with clinical implications. Journal of the American College of Cardiology 1996;28(1):168-175.

67. Kemps HM, Schep G, Hoogsteen J, Thijssen EJ, De Vries WR, Zonderland M, Doevendans P. Oxygen uptake kinetics in chronic heart failure: clinical and physiological aspects. Netherlands heart journal : monthly journal of the Netherlands Society of Cardiology and the Netherlands Heart Foundation 2009;17(6):238-244.

68. Thompson RB, Tomczak CR, Haykowsky MJ. Evaluation of Cardiac, Vascular, and Skeletal Muscle Function With MRI: Novel Physiological End Points in Cardiac Rehabilitation Research. The Canadian journal of cardiology 2016;32(10S2):S388-S396.

69. Hernando D, Kellman P, Haldar JP, Liang ZP. Robust water/fat separation in the presence of large field inhomogeneities using a graph cut algorithm. Magnetic resonance in medicine 2010;63(1):79-90.

70. de Rochefort L, Brown R, Prince MR, Wang Y. Quantitative MR susceptibility mapping using piece-wise constant regularized inversion of the magnetic field. Magnetic resonance in medicine 2008;60(4):1003-1009.

71. Wehrli FW, Fan AP, Rodgers ZB, Englund EK, Langham MC. Susceptibility-based time-resolved whole-organ and regional tissue oximetry. NMR in biomedicine 2016.

72. Li C, Langham MC, Epstein CL, Magland JF, Wu J, Gee J, Wehrli FW. Accuracy of the cylinder approximation for susceptometric measurement of intravascular oxygen saturation. Magnetic resonance in medicine 2012;67(3):808-813.

73. Karampinos DC, Yu H, Shimakawa A, Link TM, Majumdar S. Chemical shift-based water/fat separation in the presence of susceptibility-induced fat resonance shift. Magnetic resonance in medicine 2012;68(5):1495-1505.

74. Liu Y, Pu Y, Fox PT, Gao JH. Quantification of dynamic changes in cerebral venous oxygenation with MR phase imaging at 1.9 T. Magnetic resonance in medicine 1999;41(2):407-411.

75. Langham MC, Wehrli FW. Simultaneous mapping of temporally-resolved blood flow velocity and oxygenation in femoral artery and vein during reactive hyperemia. Journal of cardiovascular magnetic resonance : official journal of the Society for Cardiovascular Magnetic Resonance 2011;13:66.

76. Jain V, Abdulmalik O, Propert KJ, Wehrli FW. Investigating the magnetic susceptibility properties of fresh human blood for noninvasive oxygen saturation quantification. Magnetic resonance in medicine 2012;68(3):863-867.

77. Hernando D, Levin YS, Sirlin CB, Reeder SB. Quantification of liver iron with MRI: state of the art and remaining challenges. Journal of magnetic resonance imaging : JMRI 2014;40(5):1003-1021.

78. Duyn JH, van Gelderen P, Li TQ, de Zwart JA, Koretsky AP, Fukunaga M. High-field MRI of brain cortical substructure based on signal phase. Proceedings of the National Academy of Sciences of the United States of America 2007;104(28):11796-11801.

79. Hernando D, Liang ZP, Kellman P. Chemical shift-based water/fat separation: a comparison of signal models. Magnetic resonance in medicine 2010;64(3):811-822.

80. Sun H, Kate M, Gioia LC, Emery DJ, Butcher K, Wilman AH. Quantitative susceptibility mapping using a superposed dipole inversion method: Application to intracranial hemorrhage. Magnetic resonance in medicine 2016;76(3):781-791.

81. Salomir R, De Senneville BD, Moonen CTW. A fast calculation method for magnetic field inhomogeneity due to an arbitrary distribution of bulk susceptibility. Concept Magn Reson B 2003;19B(1):26-34.

82. Elkady AM, Sun H, Wilman AH. Importance of extended spatial coverage for quantitative susceptibility mapping of iron-rich deep gray matter. Magnetic resonance imaging 2016;34(4):574-578.

83. Myronenko A, Song XB. Intensity-Based Image Registration by Minimizing Residual Complexity. Ieee T Med Imaging 2010;29(11):1882-1891.

84. Gold GE, Han E, Stainsby J, Wright G, Brittain J, Beaulieu C. Musculoskeletal MRI at 3.0 T: relaxation times and image contrast. AJR American journal of roentgenology 2004;183(2):343-351.

85. Blaak E. Gender differences in fat metabolism. Current opinion in clinical nutrition and metabolic care 2001;4(6):499-502.

86. Langham MC, Magland JF, Floyd TF, Wehrli FW. Retrospective correction for induced magnetic field inhomogeneity in measurements of large-vessel hemoglobin oxygen saturation by MR susceptometry. Magnetic resonance in medicine 2009;61(3):626-633.

87. Thompson RB, Pagano JJ, Mathewson KW, Paterson I, Dyck JR, Kitzman DW, Haykowsky MJ. Differential Responses of Post-Exercise Recovery of Leg Blood Flow and Oxygen Uptake Kinetics in HFpEF versus HFrEF. PloS one 2016;11(10):e0163513.

88. Bassett DR, Jr., Howley ET. Limiting factors for maximum oxygen uptake and determinants of endurance performance. Medicine and science in sports and exercise 2000;32(1):70-84.

89. Haykowsky M, Brubaker P, Kitzman D. Role of physical training in heart failure with preserved ejection fraction. Current heart failure reports 2012;9(2):101-106.

90. Ozyener F, Rossiter HB, Ward SA, Whipp BJ. Influence of exercise intensity on the on- and off-transient kinetics of pulmonary oxygen uptake in humans. The Journal of physiology 2001;533(Pt 3):891-902.

91. Weatherburn MW, Stewart BJ, Logan JE, Walker CB, Allen RH. A survey of hemoglobin values in Canada. Canadian Medical Association journal 1970;102(5):493-498.

92. Jendzjowsky NG, Tomczak CR, Lawrance R, Taylor DA, Tymchak WJ, Riess KJ, Warburton DE, Haykowsky MJ. Impaired pulmonary oxygen uptake kinetics and reduced peak aerobic power during small muscle mass exercise in heart transplant recipients. Journal of applied physiology 2007;103(5):1722-1727.

93. Bangsbo J, Hellsten Y. Muscle blood flow and oxygen uptake in recovery from exercise. Acta physiologica Scandinavica 1998;162(3):305-312.

94. Pavia L, Myers J, Cesare R. Recovery kinetics of oxygen uptake and heart rate in patients with coronary artery disease and heart failure. Chest 1999;116(3):808-813.

95. Tanabe Y, Takahashi M, Hosaka Y, Ito M, Ito E, Suzuki K. Prolonged recovery of cardiac output after maximal exercise in patients with chronic heart failure. Journal of the American College of Cardiology 2000;35(5):1228-1236.

96. Wehrli FW, Fan AP, Rodgers ZB, Englund EK, Langham MC. Susceptibility-based time-resolved whole-organ and regional tissue oximetry. NMR in biomedicine 2017;30(4).

97. Billett HH. Hemoglobin and Hematocrit. In: Walker HK, Hall WD, Hurst JW, editors. Clinical Methods: The History, Physical, and Laboratory Examinations. 3rd ed. Boston; 1990.

98. Hopkins JA, Wehrli FW. Magnetic susceptibility measurement of insoluble solids by NMR: magnetic susceptibility of bone. Magnetic resonance in medicine 1997;37(4):494-500.

99. Wang Y, Yu Y, Li D, Bae KT, Brown JJ, Lin W, Haacke EM. Artery and vein separation using susceptibility-dependent phase in contrast-enhanced MRA. Journal of magnetic resonance imaging : JMRI 2000;12(5):661-670.

100. Haacke EM, Tang J, Neelavalli J, Cheng YC. Susceptibility mapping as a means to visualize veins and quantify oxygen saturation. Journal of magnetic resonance imaging : JMRI 2010;32(3):663-676.

101. Fan AP, Bilgic B, Gagnon L, Witzel T, Bhat H, Rosen BR, Adalsteinsson E. Quantitative oxygenation venography from MRI phase. Magnetic resonance in medicine 2014;72(1):149-159.